JCI insight

KLF11 protects against abdominal aortic aneurysm through inhibition of endothelial cell dysfunction

Guizhen Zhao, … , Eugene Chen, Jifeng Zhang

JCI Insight. 2021. https://doi.org/10.1172/jci.insight.141673.

Research In-Press Preview Vascular biology

Graphical abstract

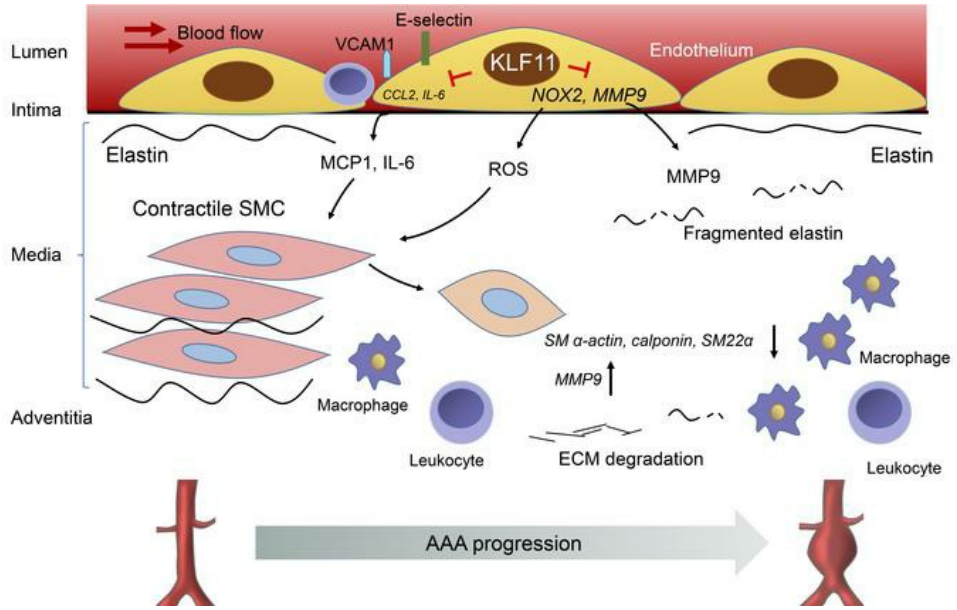

KLF11 protects against abdominal aortic aneurysm through inhibition of endothelial cell dysfunction

Guizhen Zhao[1], Ziyi Chang[1,2], Yang Zhao[1], Yanhong Guo[1], Haocheng Lu[1], Wenying Liang[1], Oren Rom[1], Huilun Wang[1], Jinjian Sun[1,3], Tianqing Zhu[1], Yanbo Fan[1,4], Lin Chang[1], Bo Yang[5], Minerva T. Garcia-Barrio[1], Y. Eugene Chen[1,5] and Jifeng Zhang[1]

Affiliations: [1]Department of Internal Medicine, University of Michigan Medical Center, Ann Arbor, MI 48109; [2]Department of Pathology, China-Japan Friendship Hospital, Beijing 100029, China ; [3]Department of Cardiovascular Medicine, the Second Xiangya Hospital, Central South University, Changsha, Hunan 410011, China; [4]Department of Cancer Biology, College of Medicine, University of Cincinnati, Cincinnati, OH 45267; [5]Department of Cardiac Surgery, University of Michigan Medical Center, Ann Arbor, MI 48109.

Corresponding Authors:

Jifeng Zhang, PhD, Department of Internal Medicine, University of Michigan Medical Center, NCRC Bldg26-357S. 2800 Plymouth Rd, Ann Arbor, MI 48109, Email: jifengz@umich.edu

Y. Eugene Chen, MD, PhD, Department of Internal Medicine, University of Michigan Medical Center, NCRC Bldg26-361S. 2800 Plymouth Rd, Ann Arbor, MI 48109, Email: echenum@umich.edu

The authors have declared that no conflict of interest exists.

Abstract

Abdominal aortic aneurysm (AAA) is a life-threatening degenerative vascular disease. Endothelial cell (EC) dysfunction is implicated in AAA. Our group recently demonstrated that Krüppel-like factor 11 (KLF11) plays an essential role in maintaining vascular homeostasis, at least partially through inhibition of EC inflammatory activation. However, the functions of endothelial KLF11 in AAA remain unknown. Here we found that endothelial KLF11 expression was reduced in the ECs from human aneurysms and was time-dependently decreased in the aneurysmal endothelium from both elastase- and *Pcsk9*/AngII-induced AAA mouse models. KLF11 deficiency in ECs markedly aggravated AAA formation, whereas EC-selective KLF11 overexpression significantly inhibited AAA formation. Mechanistically, KLF11 not only inhibited the EC inflammatory response but also diminished MMP9 expression and activity and reduced NADPH oxidase 2-mediated production of reactive oxygen species in ECs. In addition, KLF11-deficient ECs induce smooth muscle cell dedifferentiation and apoptosis. Overall, we established endothelial KLF11 as a novel factor protecting against AAA and a potential target for intervention in aortic aneurysms.

Introduction

Abdominal aortic aneurysm (AAA) is an irreversible degenerative disease, and its rupture has a mortality rate up to 90% (1, 2). The risk factors for AAA include age, male sex, smoking, hypertension, and atherosclerosis (1, 2). AAA develops because of a combination of vascular inflammation, excessive oxidative stress, and maladaptive aortic wall remodeling (2, 3). At present, only 10% of the patients are eligible for open surgical repair or invasive endovascular aneurysm repair, while drug-based therapies are still lacking (1, 3). There is an urgent need for a better understanding of the mechanisms underlying AAA development to help design novel, non-invasive therapeutic approaches.

Healthy endothelium is critical in maintaining vascular homeostasis (4, 5) through regulation of vascular tone, cellular adhesion, and VSMC homeostasis. However, prolonged exposure to cardiovascular risk factors, like smoking, hyperlipidemia, and pro-inflammatory factors, induces EC dysfunction and subsequently exacerbates vascular diseases, such as vascular inflammation (6) and atherosclerosis (5). ECs can also increase oxidative stress in the vessel wall by impaired nitric oxide bioavailability due to endothelial dysfunction and NADPH oxidase (NOX) upregulation (7). Moreover, endothelial dysfunction has been found to trigger vascular remodeling by releasing proteases or recruiting immune cells into the medial layer (8, 9). Current evidence (10, 11) supports the notion that pathological changes in ECs are likely essential steps to initiate the process of AAA formation. Therefore, investigation of EC dysfunction and the interaction between the endothelium and medial SMCs during AAA development may provide a deeper understanding of AAA pathology towards novel targeted interventions.

Krüppel-like factors, a family of zinc-finger containing transcription factors, have been implicated in many biological processes, including cell proliferation, differentiation and apoptosis (12, 13). KLF11 is a member of the KLF family with high expression in various human tissues, including

the vasculature (12). KLF11 is a vasoprotective factor and plays an essential role in maintaining vascular homeostasis (12, 14, 15). Moreover, our prior studies demonstrated that KLF11 cooperates with peroxisome proliferator-activated receptor-γ to reduce ischemic cerebral vascular endothelium damage (16) and inhibits EC inflammatory activation in the presence of pro-inflammatory stimuli (14). Noteworthy, despite emerging data from clinical and animal studies suggesting that EC dysfunction is also highly associated with AAA, the potential effect and underlying mechanism of endothelial KLF11 in AAA development remains to be addressed. Consequently, in the present study, we sought to define whether KLF11 has a protective role in AAA formation by improving endothelial cell functions and contributing to VSMC homeostasis.

Results

KLF11 is reduced in Aneurysmal Endothelium

To explore the possible relationship between KLF11 and AAA, we adopted two distinct murine AAA models (17-19): the elastase-induced AAA model and the *Pcsk9*/AngII-induced AAA model. In the elastase model (Fig. 1A-B), the progressive increase in the internal diameter of the infrarenal aorta was directly associated with a time-dependent reduction in endothelial KLF11 expression as assessed by *en face* immunofluorescence staining (Fig. 1C). The progressive down-regulation of KLF11 was mirrored in the endothelium of the suprarenal abdominal aortas after AngII-infusion (Fig. 1D-E). Those findings were consistent with the observation that the protein abundance of KLF11 is significantly reduced in the endothelial cells of aortic samples from human aortic aneurysms (Fig. 1F and Supplementary Table 1). Thus, these results indicate that KLF11 downregulation is involved in the pathology of AAA.

Endothelial KLF11 Deficiency Aggravates AAA Formation

To study the role of KLF11 in ECs during AAA development *in vivo*, we generated EC-specific *Klf11* knockout (*Klf11*^{ECKO}) mice by cross-breeding floxed-*Klf11* mice (*Klf11*$^{f/f}$) with *Tie2*-Cre mice (Supplementary Fig. 1A). The *Klf11* knockout in ECs was determined by Western blot and qPCR, and no significant differences in the expression of other *Klfs* were noted (Supplementary Fig. 1B-C). Next, 8-week-old male *Klf11*^{ECKO} (n=15) and littermate *Klf11*$^{f/f}$ (n=13) mice were subjected to *Pcsk9*/AngII-induced AAA model (Fig. 2A). We observed 1 out of 13 (7.7%) in the *Klf11*$^{f/f}$ group and 1 out of 15 (6.7%) in the *Klf11*^{ECKO} group died due to rupture of AAA. The survival rate, body weight, blood pressure, and plasma lipid profiles were comparable between the two groups (Supplementary Fig. 1D-G). Meanwhile, AngII infusion did not impact the endothelium integrity assessed by immunofluorescence staining of two EC markers, CD31 and VE-cadherin, in the AAA region (Supplementary Fig. 1H). Nevertheless, endothelial *Klf11*

deficiency markedly increased the incidence of AAA (86.67%) and the maximal diameters of the suprarenal abdominal aorta (1.872±0.175 mm) compared with those in *Klf11*$^{f/f}$ mice (AAA incidence of 46.15% and maximal diameter of 1.383±0.067 mm) after AngII infusion (Fig. 2B-D). Endothelial *Klf11* knockout markedly enhanced elastin degradation and matrix metallopeptidase 9 (MMP9) expression in the aortic sections, particularly in the endothelium (Fig. 2E and Supplementary Fig. 1I). Moreover, leukocyte ($CD45^+$) and macrophage ($Mac2^+$) infiltration to the aortic wall and the concentration of plasma MCP-1 and IL-6 were markedly increased in *Klf11*^{ECKO} mice compared with *Klf11*$^{f/f}$ mice (Fig. 2F-G). Additionally, endothelial *Klf11* deficiency significantly increased VSMC apoptosis assessed by TUNEL staining and superoxide production assessed by dihydroethidium (DHE) staining in the aortic wall of *Pcsk9*/AngII-induced AAA (Fig. 2H-I).

We also performed elastase-induced infrarenal AAA on 8 to 12-week-old male *Klf11*$^{f/f}$ and *Klf11*^{ECKO} mice. Fourteen days after elastase-exposure, the body weight, blood pressure, plasma lipid profiles, and MCP-1 were comparable between the two groups (Supplementary Fig. 2A-D). Consistent with our findings in the *Pcsk9*/AngII-induced AAA model, *Klf11*^{ECKO} mice exhibited enhanced abdominal aortic enlargement, elastin degradation, as well as leukocyte and macrophage accumulation in the aortic walls, compared with *Klf11*$^{f/f}$ mice (Supplementary Fig. 2E-H). These data support that loss of KLF11 promotes AAA.

KLF11 Overexpression in ECs Attenuates AAA Formation

To further evaluate the protective role of endothelial KLF11 in AAA, we generated EC-selective *KLF11* transgenic mice (*Tie2-KLF11* Tg) and validated KLF11 overexpression in ECs through western blot (Supplementary Fig.3A-B). Next, we performed the *Pcsk9*/AngII-induced AAA model on male *Tie2-KLF11* Tg mice and their littermate wild type (WT) mice. No significant differences were found regarding survival rate (3 mice in WT group and 2 mice in *Tie2-KLF11*

Tg group died due to rupture of the thoracic aorta), systolic blood pressure, body weight, and plasma lipid profiles between the two groups (Supplementary Fig. 3C-F). However, KLF11 overexpression in ECs significantly reduced AAA incidence (WT, 60% *vs. Tie2-KLF11* Tg, 10%, Fig. 3A-B). Concomitantly, the maximal suprarenal aortic diameter (WT, 1.841±0.137 mm *vs. Tie2-KLF11* Tg, 1.172±0.063 mm), elastin degradation, MMP9 expression in the endothelium, and leukocyte and macrophage accumulation in the aortic wall were significantly attenuated in *Tie2-KLF11* Tg mice compared with WT mice (Fig.3C-E and Supplementary Fig. 3G). Additionally, KLF11 overexpression in ECs significantly reduced VSMC apoptosis in the aortic wall (Fig. 3F).

Next, the elastase-induced AAA model was also performed on the male *Tie2-KLF11* Tg mice and WT mice. There was no noticeable difference in body weight, blood pressure, plasma lipid profiles, MCP-1, and IL-6 between the two groups (Supplementary Fig. 4A-D). Meanwhile, elastase exposure did not destroy the endothelium integrity evidenced by immunofluorescence staining of CD31 and VE-cadherin (Supplementary Fig. 4E). However, and consistent with the *Pcsk9*/AngII model, KLF11 overexpression in ECs significantly reduced elastase-induced AAA incidence (WT, 90% vs. *Tie2-KLF11* Tg, 20%), the abdominal aortic enlargement, elastin degradation, MMP9 expression in the endothelium, and leukocyte and macrophage accumulation as well as the superoxide production in the aortic wall (Supplementary Fig. 4F-L). The above findings indicate that endothelial KLF11 protects against murine AAA development.

Bone Marrow-derived KLF11 does not affect AAA formation

To exclude the effects of KLF11 loss- or gain-of-function in blood cells (monocytes, lymphocytes, etc.) in AAA formation, bone marrow transplant (BMT) experiments were performed as described previously (20, 21). Briefly, the bone marrow cells isolated from *Klf11*$^{f/f}$ and *Klf11*^{ECKO} mice were transplanted to irradiated WT mice, and the elastase-induced AAA

model was performed on those mice (Supplementary Fig. 5A-B). Fourteen days after elastase exposure, the body weight, blood pressure, and plasma lipid profiles were comparable between the two groups of recipient mice (Supplementary Fig. 5C-E). The KLF11-deficient bone marrow cells do not impact the AAA incidence, abdominal aortic enlargement, elastin degradation, and inflammatory cell accumulation in the aortic wall (Supplementary Fig. 5F-J). Those findings were further confirmed in another BMT experiment (Supplementary Fig. 6). The WT and *Tie2-KLF11* Tg mice transplanted with WT bone marrow were subjected to the elastase-induced AAA model. Two weeks after elastase exposure, there were no differences between the two groups in body weight, blood pressure, plasma lipid profiles, MCP-1, and IL-6 (Supplementary Fig. 6A-D). The AAA incidence, abdominal aortic dilation, elastin degradation, as well as the leukocyte and macrophage accumulation in the aortic wall were greatly decreased in the *Tie2-KLF11* Tg mice transplanted with WT bone marrow compared with WT mice transplanted with WT bone marrow (Supplementary Fig. 6E-I). Collectively, these data indicate that increase in endothelial KLF11, rather than myeloid KLF11, is responsible for the KLF11 protective effects in AAA.

KLF11 Suppresses Endothelial Cell Inflammatory Activation

Vascular inflammation is a fundamental element in the development of AAA (2, 3). ECs play an important role in vascular inflammation by expressing pro-inflammatory molecules (11). Our previous work demonstrated that KLF11 suppresses EC activation via NFκB signaling (14). To unravel the protective mechanisms of KLF11 against endothelial dysfunction, we performed RNA sequencing analysis of human aortic endothelial cells (HAECs) with *KLF11* knockdown using adenovirus-short hairpin RNA (Ad-sh*KLF11*), followed by gene set enrichment analysis (Supplementary Table 2). Of note, the pathways for inflammatory response (normalized enrichment score [NES]=1.31, FDR q-value=0.161) and TNF-α signaling *via* NF-κB (NES=1.35, FDR q-value=0.118) were enriched amongst the up-regulated pathways in HAECs infected with

Ad-sh*KLF11* (Supplementary Fig. 7A), indicating that the inflammatory response is activated upon *KLF11* knockdown in ECs. The upregulation of pro-inflammatory genes (Supplementary Fig. 7B and Supplementary Table 3), such as VCAM1, E-selectin (encoded by *SELE*), was further validated through qPCR and Western blot. Consistently, *KLF11* knockdown significantly enhanced the expression of those pro-inflammatory genes under TNF-α stimulation (Supplementary Fig. 7C-D). Conversely, adenovirus-mediated *KLF11* overexpression (Ad-*KLF11*) significantly inhibited TNF-α-induced expression of those pro-inflammatory genes (Supplementary Fig. 7E-F). In addition, *KLF11* knockdown enhanced MCP-1 and IL-6 secretion from the TNF-α-stimulated HAECs, whereas *KLF11* overexpression decreased TNF-α-induced secretion of MCP-1 and IL-6 (Supplementary Fig. 7G-H). Consistent with the reduced secretion of MCP-1 and IL-6, the conditioned medium from *KLF11*-overexpressing HAECs inhibited macrophage migration (Supplementary Fig. 7I). Additionally, leukocyte-EC adhesion assays showed that knockdown of *KLF11* in ECs using small interfering RNA (si*KLF11*) markedly increased TNF-α-mediated leukocyte adhesion to EC, whereas *KLF11* overexpression in ECs significantly reduced the leukocyte-EC adhesion, concomitant with the changes of VCAM1, ICAM1, and E-selectin in ECs (Supplementary Fig. 7K-J). Taken together, our data demonstrate an inhibitory role of KLF11 on the migration and recruitment of inflammatory cells to ECs *in vitro* by modulating the expression and secretion of pro-inflammatory cytokines and adhesion molecules in ECs.

KLF11 Inhibits MMP9 Expression in ECs

Increased expression of MMPs was observed in human and animal AAA tissues (22, 23). Consistently, the *in vivo* data showed that endothelial *Klf11* deficiency significantly enhanced MMP9 expression, whereas *KLF11* overexpression in ECs markedly reduced MMP9 expression in the endothelium from AAA models (Supplementary Fig. 1H, 3G and 4L). Moreover, gene set

enrichment analysis (Supplementary Table 4) upon *KLF11* knockdown revealed that the pathways of membrane protein proteolysis (NES=1.60, FDR q-value=0.292) and metalloexopeptidase activity (NES=1.48, FDR q-value=0.487) were enriched in HAECs infected with Ad-sh*KLF11* (Fig. 4A), accompanied by upregulation of multiple proteinases, such as *MMP2*, *MMP9* and *ADAMTS3* (a disintegrin and metalloproteinase with thrombospondin motifs 3) (Fig. 4B and Supplementary Table 5). Next, we validated the expression of *MMP2*, *MMP9*, *MMP13,* and *MMP14* in HAECs using qPCR. *KLF11* knockdown enhanced while *KLF11* overexpression reduced TNF-α-induced expression of *MMP9* (Fig. 4C-D). Additionally, we noticed that inflammatory stimulus with TNF-α (2ng/ml) increased the activation of MMP9 assessed by gelatin zymography in the EC conditioned medium, while *KLF11* knockdown further enhanced TNF-α-induced activation of MMP9 (Fig. 4E). In contrast, *KLF11* overexpression reduced the activation of MMP9 (Fig. 4F). Next, chromatin immunoprecipitation (ChIP) assay performed in the HAECs demonstrated that KLF11 binds to the putative KLF binding site (-594 to -574) upstream of the *MMP9* transcription start site (Fig. 4G). Furthermore, we generated a luciferase reporter construct containing the -693 to +5 region of the human *MMP9* promoter. In HAECs transfected with the *MMP9* reporter construct, *KLF11* overexpression significantly reduced the luciferase activity under TNF-α stimulation (Fig. 4H). Multiple inflammatory genes and MMPs are direct targets of NF-κB signaling pathway (14, 24, 25). Our prior study demonstrated that KLF11 inhibits NF-κB signaling pathway *via* interaction with P65 (14). Consistently, we found that KLF11 overexpression reduced TNF-α-induced luciferase activity using a reporter containing NF-κB response elements (Supplementary Fig. 8A). Moreover, administration of NF-κB pathway inhibitor (BAY11-7082, which inhibits the phosphorylation of IκBα) can abolish the effect of KLF11 knockdown on MMP9 expression in response to TNF-α in HAECs (Supplementary Fig. 8B). Using ChIP assay, we found that KLF11 overexpression reduces the binding of P65 to the NF-κB binding site located at (-627)-(-613) within *MMP9* promoter, which are close to the putative KLF11 binding sites (-594 to -574)

(Supplementary Fig. 8C). Collectively, our data indicate that KLF11 inhibition of MMP9 expression at the transcriptional level involves both NF-κB pathway-dependent and independent mechanisms.

KLF11 Suppresses Endothelial Oxidative Stress through Inhibition of NOX2

Excessive ROS (eg. superoxide, hydroxyl radical) has been implicated in the pathogenesis of AAA (26, 27). Consistently, superoxide was increased in the aortic wall of *Klf11*^{ECKO} mice in the AAA region, whereas KLF11 overexpression in ECs reduced superoxide production (Fig. 2I and Supplementary Fig. 4K). Interestingly, without stimuli, *KLF11* knockdown did not affect superoxide production in HAECs *in vitro* (Fig. 5A). Multiple stimuli have been shown to induce ROS production in ECs, such as TNF-α and AngII (28, 29). Of note, *KLF11* knockdown significantly increased superoxide production in ECs under those stimuli (Fig. 5A). Accordingly, *KLF11* overexpression decreased TNF-α- and AngII-induced superoxide production (Fig. 5B). These results indicate that under pathological conditions, KLF11 deficiency increased endothelial superoxide production.

NOXs are the major source of superoxide production in human and animal vasculature (30, 31), and ECs can express four isoforms, v.g. NOX1, NOX2, NOX4, and Nox5 (28, 32). We found that *KLF11* knockdown markedly increased *NOX2* expression in HAECs under TNF-α and AngII treatment, without any significant effects on the expression of *NOX1*, *NOX4,* and *NOX5* (Supplementary Fig. 9A and Fig. 5C-D). Conversely, *KLF11* overexpression reduced NOX2 expression in HAECs under the same stimuli (Fig. 5E). Additionally, the increased superoxide production directly associated with KLF11 deficiency in the presence of TNF-α or AngII was abrogated by *NOX2* knockdown (si*NOX2*) (Fig. 5F and Supplementary Fig. 9B). Accordingly, DHE staining demonstrated that knockdown of *NOX2* or treatment with the NOX2 inhibitor (GSK2795039, NOX2i, 1μM) significantly attenuated the increase in superoxide production

associated with KLF11 down-regulation (Fig. 5G-H). Bioinformatics analysis revealed a potential KLF binding site (-645 to -663bp) upstream of the *NOX2* transcription start site. ChIP assay demonstrated that KLF11 binds to the promoter of *NOX2* to inhibit its expression (Fig. 5I). Of note, knockdown of *KLF11* can upregulate *NOX2* expression both under basal conditions and in response to TNF-α. However, inhibition of NF-κB activation *via* BAY11-7082 could not abolish the effect of KLF11 on *NOX2* expression in the presence of TNF-α (Supplementary Fig. 9C). Moreover, overexpression of *KLF11* did not affect the binding of P65 to the potential NF-κB binding site (-712 to -698bp), close to the KLF11 binding site (-645 to -663bp) within the *NOX2* promoter (Supplementary Fig. 9D). These data suggest that KLF11 inhibits NOX2 expression at the transcriptional level mainly through directly binding to a consensus sequence within its promoter, particularly under basal conditions.

In human and animal AAAs, oxidative stress is a crucial trigger for vascular inflammation and MMP-dependent proteolysis (26, 27). Our data showed that enhanced expression of inflammatory molecules, such as *VCAM1*, *SELE*, *CCL2,* and *IL-6*, in HAECs with *KLF11* knockdown and stimulated with TNF-α, could be attenuated by *NOX2* knockdown (Supplementary Fig. 8B). Recently, cyclophilin A (CypA) has emerged as a ROS-sensitive secreted cytokine in *Pcsk9*/AngII-induced aortic aneurysm and dissection (28). We found that *KLF11* knockdown significantly increased *CypA* expression in HAECs, and *CypA* expression was further enhanced upon TNF-α stimulation in combination with *KLF11* knockdown (Supplementary Fig. 8C). Similarly, knockdown of *NOX2* completely abolished the increase in *CypA* expression induced by *KLF11* knockdown (Supplementary Fig. 8C). Furthermore, knockdown of *NOX2* impaired the upregulation of *MMP9* in HAECs with *KLF11* knockdown (Supplementary Fig. 8D)

Taken together, these results indicate that KLF11 inhibits NOX2 expression at the transcriptional level by directly binding to the *NOX2* promoter to preserve EC homeostasis

while, under pathological conditions, KLF11 downregulation increases endothelial ROS production mediated, in part, through upregulation of NOX2, thus contributing to EC dysfunction.

KLF11 expression in EC is critical for maintaining the SMC contractile phenotype

With the identification of increased SMC apoptosis within the aortic wall of *Klf11*^{ECKO} mice in the AAA model, we next sought to determine whether EC dysfunction induced by KLF11 deficiency was involved in regulating VSMC phenotypic transformation and apoptosis. First, we used the conditioned media from HAECs (EC-CM) with either *KLF11* knockdown or overexpression, subsequently treated with or without TNF-α (2ng/ml), to culture human aortic smooth muscle cells (HASMCs) for 24h. The EC-CM from HAECs treated with vehicle did not affect SMC contractile genes expression (Fig. 6A-D). Of note, HASMCs grown in the EC-CM from HAECs with *KLF11* knockdown and treated with TNF-α, displayed decreased expression of SMC contractile markers, such as smooth muscle alpha-actin (SMA), calponin, and smooth muscle 22 alpha (SM22α), and increased MMP9 expression, with no change in the expression of pro-inflammatory cytokines, such as MCP-1 and IL-6 (Fig. 6A-B). In contrast, the EC-CM from HAECs with *KLF11* overexpression and TNF-α stimulation significantly increased the expression of SMC contractile markers and reduced MMP9 expression relative to the EC-CM from Ad-*GFP*-infected HACECs in the same conditions (Fig. 6C-D).

Furthermore, the EC-CM from TNF-α-stimulated HAECs with *KLF11* knockdown significantly increased HASMC apoptosis, as assessed by TUNEL staining, compared with the EC-CM from siControl transfected HACECs stimulated with TNF-α (Fig. 6E). Additionally, we determined the expression of the apoptosis regulator BCL2 associated X protein (BAX) using a co-culture system (Fig. 6F). After 24h of co-culture in fresh opti-MEM with HAECs that had been transfected with si*KLF11* 48h earlier, and stimulated with TNF-α (2ng/ml) for 1h, HASMCs demonstrated increased BAX protein abundance in comparison with HASMCs co-cultured with

HAECs transfected with siControl and treated with TNF-α (Fig. 6G). In contrast, in co-culture with TNF-α-treated HAECs overexpressing *KLF11*, HASMCs showed decreased expression of BAX (Fig. 6H). Notably, silencing of *NOX2* in ECs with *KLF11* knockdown and TNF-α stimulation could partially reverse the effect of KLF11 knockdown (Fig. 6A, B, and G). Taken together, our data indicate that KLF11-expression in ECs is required for maintaining the VSMC contractile phenotype and preventing VSMC apoptosis, two essential VSMC phenotypes involved in AAA.

Discussion

AAA is a fatal arterial disease, which usually remains asymptomatic until rupture, at which stage results in 80% mortality (3). AAA is a complex pathophysiological process, and its underlying mechanisms remain incompletely understood. In this study, we demonstrated that endothelial KLF11 acts as a vasoprotective factor against AAA through multifaceted mechanisms that include reduction of inflammatory response, inhibition of MMP9 expression, and suppression of NOX2-mediated ROS production in ECs, as well as the preservation of VSMC contractile phenotype and viability.

Vascular inflammation and excessive inflammatory cell recruitment to the vascular wall are essential factors in the initiation and progression of AAA (2, 33). The recruitment of inflammatory cells is mediated primarily by EC activation, and the consequent increased expression of pro-inflammatory molecules, such as VCAM1, E-selectin, and MCP-1 (11, 34). In particular, TNF-α-induced NF-κB activation is one of the major pathways contributing to inflammation-mediated vascular injury (9, 35). Our previous study demonstrated that KLF11 reduced TNF-α-induced expression of adhesion molecules *via* inhibition of the NF-κB signaling pathway (14). However, the specific role of KLF11 in AAA remained unknown. In the current study, we uncovered that *Klf11* depletion in ECs enhanced leukocyte and macrophage accumulation in the aortic wall, both in *Pcsk9*/AngII- and elastase-induced AAA models, concomitant with increased expression of adhesion molecules and cytokines in ECs and increased monocyte adhesion in the presence of inflammatory stimuli. Furthermore, the protective role of EC-specific KLF11 in AAA was determined using BMT experiments and elastase-induced AAA model, to exclude a protective contribution of monocytic KLF11 to reduced AAA. Our study is the first to reveal a protective role of KLF11 in AAA formation through anti-inflammatory effects on ECs and its homeostatic consequences on VSMCs.

The aortic ECM degradation by proteases, including MMPs (36), ADAMTSs (37) and cysteine proteases (36, 38), is a crucial step in the formation and progression of AAA, and these proteases are increased in the aortic wall from patients with AAA (37). However, the specific role of the endothelial MMPs in AAA progression remains poorly understood. Our observation that MMP9 expression was significantly and specifically increased in ECs from EC-specific *Klf11* knockout mice in both AAA models used here indicates that endothelial KLF11 plays a crucial role in the regulation of MMP9 production by ECs. Moreover, we found that, under the pro-inflammatory stimuli, KLF11 not only inhibits MMP9 expression but also reduces the activation of MMP9 in ECs. Recently, endothelial MMP9 was described as a trigger of the inflammatory response in AAA (8). Moreover, ECM fragments proteolytically generated by MMPs also show bioactive properties and promote the recruitment of inflammatory cells, such as macrophages and T cells (39-41). Subsequently, the recruited inflammatory cells produce more inflammatory cytokines and proteases, which potentiate the inflammatory response and vascular injury. In this context, our finding identifies EC expression of MMP9 as a potentially critical mechanism that regulates vascular remodeling and inflammation, essential to AAA initiation and progression.

Oxidative stress is a leading cause of cardiovascular diseases in general and causes vessel damage due to increased production or impaired clearance of ROS (42, 43). Excessive ROS act as destructive agents affecting DNA and proteins, leading to inflammation and tissue injury (44, 45). In vascular ECs, the major sources of ROS are the NAPDH oxidases (7, 42), and NOX2 is the main source of ROS production in response to pathological stimuli, such as TNF-α and AngII (28, 29, 46). Recently, EC-specific NOX2 overexpression and the resulting heightened ROS production were shown to increase the susceptibility to *Pcsk9*/AngII-induced aortic dissection (28), consistent with the increase of NOX2 abundance found in human aortic aneurysm tissues (27). However, relatively little is known about the mechanisms that regulate NOX2 expression in ECs. In this study, we show for the first time that deficiency of endothelial

KLF11 results in substantial upregulation of NOX2 and ROS production associated with endothelial *Klf11* knockout aggravation of the AAA pathogenesis. We show that *NOX2* knockdown reduced ROS production in ECs with *KLF11* knockdown, and demonstrate that KLF11 is a crucial transcriptional repressor of NOX2 expression in ECs in response to AAA-relevant stimuli, thus establishing a direct association between KLF11 downregulation and enhanced NOX2-dependent ROS production in ECs. In addition, the expression of inflammatory molecules, including VCAM1, E-selectin, MCP-1, and IL-6, were partially inhibited after knockdown of *NOX2* in ECs with *KLF11* knockdown, suggesting that endothelial oxidative stress and inflammation concurrently increase the damage to the aortic wall. Although some studies support that oxidative stress contributes to the pathogenesis of AAA (26, 27) and anti-oxidant drugs, such as vitamin E can reduce the size of AAA in pre-clinical experimental models (47), to date, no antioxidant therapy has proven effective at preventing AAA in human. Our study points towards a causative role of endothelial NOX2 in the pathogenesis of AAA in experimental models, suggesting that this oxidase could be a molecular target for the treatment of AAA.

ECs also secrete a variety of substances that affect the neighboring cells. Recent studies show that ECs regulate the functions and phenotypes of VSMCs by releasing various bioactive agents, such as microRNA (48), nitric oxide (49), and enzymes (8). In this study, we showed that VSMCs stimulated with conditioned media or co-cultured with ECs subjected to *KLF11* silencing have significantly lower expression of SMC-specific contractile markers, including smooth muscle α-actin, calponin, and SM22α, but higher expression of MMP9 and enhanced apoptosis. In addition, oxidative stress and apoptosis in ECs and medial VSMCs were markedly enhanced in the aneurysmal aortas from EC-specific *Klf11* knockout mice, suggesting that KLF11-dependent effects in ECs are essential for the interaction between ECs and VSMCs towards maintaining normal vascular physiology and structure *in vivo*. Accordingly, endothelial KLF11-deficiency leads to enhanced MMP9 production and apoptosis in VSMCs, further

weakening the vascular wall and contributing to AAA formation. CypA, a ROS-dependent factor secreted from ECs, has been recently identified to mediate VSMC activation in AngII-induced aortic dissection (28). Consistently, *KLF11* knockdown also increased *CypA* expression in ECs and *NOX2*-silencing could abolish this effect, suggesting that increased CypA in KLF11-deficient ECs may further contribute to induce VSMC phenotypic changes. The conditioned media from ECs with *KLF11* knockdown and TNF-α stimulation potentially contains a great variety of factors, such as those identified here (namely, inflammatory cytokines, MMP9, CypA and ROS), all of which can trigger or promote VSMC dedifferentiation and apoptosis. Hence, follow-up studies will focus on the systematic identification in the endothelial conditioned media of the gamut of KLF11-dependent secreted factors which may act as intermediate molecules for the KLF11-dependent effects in the crosstalk between EC and VSMC and which could serve as targets of intervention for AAA.

In summary, we define for the first time EC-specific KLF11 as a novel protective factor against AAA operating by reducing endothelial inflammation and ROS production, improving EC function and maintaining vascular homeostasis. These protective effects involve the newly identified KLF11 direct transcriptional inhibition of MMP9 and NOX2. Indeed, loss of KLF11 as AAA progresses directly allows NOX2-dependent ROS overproduction in ECs causes endothelial activation, expression of adhesion molecules, secretion of chemokines and production of ECM-degrading protease MMP9, which further amplify the vascular inflammation associated with AAA and other vascular diseases. These findings indicate that KLF11-dependent effects on ECs may define new targets for intervention in the treatment of AAA and cardiovascular disease at large.

Materials and Methods

Reagents

KLF11 antibody (X1710) was produced by Syd labs (Natick, MA). CD31 antibody (DIA-310) was purchased from Dianova (Hamburg, GER). CD45 antibody (550539) was purchased from BD Biosciences (San Jose, CA). Galectin 3 (Mac2) antibody (14-5301-85) was purchased from Thermo Fisher Scientific (Waltham, US). The antibodies for MMP9 (ab38898), alpha-smooth muscle actin (ab119952), calponin (ab46794), and SM22 alpha (ab103135) were from Abcam (Cambridge, UK). The antibodies for VE-cadherin (sc-6458), VCAM1(sc-13160), E-selectin (sc-14011), and EIF5 (sc-28309) were from Santa Cruz Biotechnology (Santa Cruz, CA). NOX2 antibody (NBP2-67680) was purchased from Novus Biologicals (Centennial, CO). The antibodies for β-actin (4967), glyceraldehyde 3-phosphate dehydrogenase (GAPDH, 5174), Flag (DYKDDDDK) tag (14793), rabbit IgG (2729), and BAX (2772) were from Cell Signaling Technology (CST, Danvers, MA). Recombinant human TNF-α (210-TA) was from R&D Systems (Minneapolis, MN) and used at 2 ng/ml to stimulate endothelial cells. Angiotensin II (AngII, H-1706) was purchased from Bachem (Vista, CA) and used at 1 μM to stimulate endothelial cells.

Cell culture

Human aortic endothelial cells (HAECs, CC-2535) from a 54-year-old male and human aortic smooth muscle cells (HASMCs, CC-2571) from a 22-year-old male were purchased from Lonza (Walkersville, MD). HAECs and HASMCs were cultured in endothelial cell growth media-2 (EGM-2, CC-3202, Lonza, Walkersville, MD) and smooth muscle cell growth medium-2 (C-22062, Promo Cell, Germany), respectively, at 37°C, 5% CO_2 in a humidified cell culture incubator. Both HAECs and HASMCs were used from passages 4-8 in all experiments. The human monocyte cell line THP-1 was purchased from ATCC (Manassas, VA) and grown in

RPMI 1640 containing 10% FBS (Thermo Fisher Scientific, Waltham, MA) and 50 mg/ml of a penicillin/streptomycin solution.

Animals and mouse AAA models

The *Klf11*$^{f/f}$ mice containing loxP sites flanking exon 3 of *Klf11* were generated at the Transgenic Core facility in the University of Michigan from *Klf11* targeted embryonic stem cells purchased from UC Davis (Davis, CA). The B6.Cg-Tg(*Tek*-Cre)1Ywa/J *(Tie2*-Cre, Stock No. 008863) mice were purchased from The Jackson Laboratory (Bar Harbor, ME). The endothelial cell-*specific* *Klf11* knockout mice (*Klf11*^{ECKO}) on the C57BL/6 background were generated by cross-breeding *Klf11*$^{f/f}$ mice with *Tie2*-Cre mice. The endothelial cell-selective *Klf11* transgenic mice (*Tie2*-*KLF11* Tg) on the C57BL/6 background were generated at the Transgenic Core facility at the University of Michigan by using a human *KLF11* ORF driven by a mouse *Tie2*-promoter. The C57BL/6J mice were purchased from The Jackson Laboratory.

The peri-adventitial elastase application (elastase)-induced AAA model was performed as previously described (17, 50). Briefly, 10- to 12-week-old male mice were anesthetized by intraperitoneal injection of a mixture of ketamine (100 mg/kg) and xylazine (5 mg/kg). The infrarenal abdominal aorta was isolated and then surrounded with a sterile gauze, previously soaked with 30μL of elastase (44 units/mL, MilliporeSigma, E1250). After 30 min incubation, the gauze was removed, and the abdominal cavity was washed twice with sterile saline before suturing.

The *Pcsk9*/Angiotensin II (AngII)-induced murine AAA model was performed as previously described (18, 19). In brief, 8- to 10-week-old male mice were injected intraperitoneally with 2X10^{11} genomic copies of adeno-associated virus (AAV, serotype 8) carrying a gain-of-function mutation of the mouse *Pcsk9* (AAV-*Pcsk9.D377Y*, Penn Vector Core at the University of Pennsylvania) and switched to a Western diet containing 0.2% cholesterol by weight (TD.88137,

Envigo, Hachensack, NJ) to induce hypercholesterolemia. Two weeks after AAV injection, mice were subcutaneously implanted with osmotic mini-pumps (Alzet, Model 2004, Cupertino, CA) to infuse AngII (Bachem, H-1706, Vista, CA) for 28 days at a releasing rate of 1500 ng/kg/min.

Fourteen days after elastase-exposure or 28 days after AngII infusion, mice were euthanized, blood was collected by ventricle puncture before-perfusion with saline and 4% paraformaldehyde through the left ventricle to remove the remaining blood, followed by isolation of the aortas for *ex vivo* measurements. The maximal external diameters of the infrarenal abdominal aortas from the elastase-induced AAA model and suprarenal abdominal aortas from the *Pcsk9/*AngII-induced AAA model were determined. Diameters larger than 50% than those of the adjacent portion were considered as AAA (51). The mice with ruptures in the thoracic aorta were excluded from the calculation of incidence of *Pcsk9*/AngII-induced AAA. The systolic blood pressure was measured by a non-invasive tail-cuff method (Visitech BP-2000, Cary, NC).

Plasma total cholesterol (TC) and triglyceride (TG) levels were measured by enzymatic kits (Wako Diagnostics, Osaka, Japan). The mice from the *Pcsk9*/AngII-induced AAA model with TC levels less than 250 mg/dl at endpoint were excluded from data analysis regardless of whether they had developed AAA. Serum MCP-1 and IL-6 levels were determined by ELISA at the Immunology Core at the University of Michigan.

En face **immunofluorescence staining**

Male C57BL/6J mice, 10-weeks old, were subjected to elastase- and *Pcsk9*/AngII-induced AAA models. After perfusion and fixation, the infrarenal abdominal aortas from mice at 0, 7 and 14 days after elastase-exposure, and suprarenal abdominal aortas from mice with AngII-infusion for 0, 7 and 14 days, were isolated and permeabilized for 10 min using a permeabilizing solution (0.1% Triton X-100 in PBS) with rocking at room temperature. After washing with PBS, the

aortas were incubated in TTBS (Tris-buffered saline with 2.5% Tween 20) with 10% normal donkey serum for 30 min with rocking at room temperature. The rabbit anti-KLF11 antibody (Syd labs, X1710, 1:50 dilution) and goat anti-VE-cadherin (Santa Cruz, sc-6458, 1:50 dilution), or normal rabbit or goat IgG in TTBS containing 10% normal donkey serum were incubated with the aortas overnight, with gentle rocking at 4°C. Alexa Fluor conjugated secondary antibodies (Jackson ImmunoResearch Laboratories) were applied for 1 hour, with rocking at room temperature. After washing three times with TTBS, the aortas were longitudinally opened to expose the endothelium. The aortas were mounted on cover glasses using ProLong™ Gold Antifade Mountant with DAPI (Invitrogen, P36935), with the endothelium facing down. Immunofluorescence images were captured with a Nikon A1 inverted confocal microscope.

Aortic Endothelial Cells from Human Patients with Aortic Aneurysm

The human samples used in this study were from the Michigan Biorepository of the University of Michigan Cardiovascular Health Improvement Project (CHIP), in the Department of Surgery at the University of Michigan. Cardiac surgeons are routinely performing surgery to collect the tissues for the CHIP initiative with patient informed consent. All the human samples in CHIP are collected with specific approval from the Human Research Protection Program and Institutional Review Boards of the University of Michigan Medical School (Hum00077616). The aortic specimens were obtained from 5 patients with aortic aneurysm undergoing open surgical aortic repair, and 4 control samples were obtained during heart transplants (Supplementary Table 1). The aortic endothelial cells from fresh specimens were gently scraped from the aortic specimens and lysed in RIPA lysis buffer (Thermo Fisher Scientific, 89901, Waltham, MA) supplemented with the cOmplete™ EDTA-free protease inhibitor cocktail (Roche, 11873580001, Penzberg, Germany) and PhosSTOP™ phosphatase inhibitor (Roche, 4906845001, Penzberg, Germany), followed by western blot.

Isolation and Culture of Mouse Pulmonary Endothelial Cells

Mouse pulmonary endothelial cells were isolated by two rounds of cell sorting using CD31 and ICAM-2 antibody coated magnetic beads as previously described (52, 53). In brief, aliquots of Dynabeads (Invitrogen, 11305) were placed on DynaMag^{TM}-Spin Magnet (Thermo Fisher, 12320D), washed with DPBS (without Ca^{2+} and Mg^{2+}) containing 0.1% BSA (0.1%BSA/DPBS) for three times according to the manufacturer's instructions and incubated with CD31 antibody (BD Pharmingen^{TM}, 553369) and ICAM2 antibody (BD Pharmingen^{TM}, 01800D) respectively overnight with rotation at 4°C. The antibody-coated beads were washed four times with 0.1%BSA/DBPS. The 4-week-old mice were anesthetized using an intraperitoneal injection of ketamine (100 mg/kg) and xylazine (5 mg/kg) and the lung lobes were aseptically excised and placed in cold isolation buffer (DMEM supplemented with 20% heat-inactivated FBS, 20 mM HEPES and 0.5 mg/ml penicillin/streptomycin). After removing the bronchi, the lung tissues were minced and digested in 2 mg/ml collagenase A (Sigma Aldrich, 10103586001) for 30 min with gentle rocking at 37°C. The digested tissue suspension was further dissociated by aspirating the suspension up and down more than 12 times with a syringe fitted with a 14G needle. The cell suspension was then pipetted through a 70 μm strainer and centrifuged at 400g for 5 min at 4°C. The cell pellets were resuspended with 0.1%BSA/DPB and incubated with the anti-CD31-coated beads (15μl beads/ml cell suspension) for 10 min with gentle rotating at room temperature. The beads and sorted endothelial cells were washed with isolation buffer five times and cultured in growth medium (DMEM supplemented with 1mol/L HEPES, 10mg/ml heparin, 50mg/ml penicillin/streptomycin, 20%FBS, 1mM sodium pyruvate, 1x non-essential amino acids solution [Gibco, 11114-050] and 20 μM L-glutamine [Gibco, 25030-081]) on a collagen I-coated T75 flask. When the cells grew to 90% confluence, the cells were detached with 0.25% trypsin-EDTA and subjected to the second round of sorting with anti-ICAM2-coated beads following equivalent steps as those for the first sorting. More than 80% of the sorted cells

are endothelial cells, as verified by vWF and VE-cadherin immunostaining. The cells were used for experiments after the culture reached about 80% confluence.

Histology

The suprarenal abdominal aortas (from the diaphragm to the right renal artery) from the AngII-induced AAA model and the infrarenal abdominal aortas from the elastase-induced AAA model were excised. The aortas were embedded in paraffin at the In-Vivo Animal Core (IVAC) from the University of Michigan. The serial sections (5μm thick, 200μm apart) were deparaffinized, rehydrated, and stained with a Verhoeff-van Gieson (VVG) staining kit (Electron Microscopy Sciences) for elastin assessment according to the manufacturers' instructions. Based on the previous report (19, 51), elastin degradation was graded as: 1, < 25% degradation; 2, 25% to 50% degradation; 3, 50% to 75% degradation; or 4, > 75% degradation.

For immunostaining, the rehydrated sections were boiled in Citrate Buffer at pH 6.0 (Invitrogen, 00-5000) for epitope retrieval for 15 min. After blocking with 5% donkey serum in PBS for 1 hour at room temperature, the sections were incubated with primary antibody against CD45 (BD Biosciences, 550539,1:50), Mac2 (Thermo-Fisher Scientific, 14-5301-85, 1:100), MMP9 (Abcam, ab38898, 1:100) or VE-cadherin (Santa Cruz, sc-6458, 1:50) at 4°C overnight. After washing with PBS, the sections were incubated with Alexa Fluor conjugated secondary antibody (Jackson ImmunoResearch Laboratories) for 1 hour at room temperature. The negative controls were sections incubated with species-matched IgG. Slides were mounted with ProLong™ Gold Antifade Mountant with DAPI (Invitrogen, P36935) before image collection with an Olympus DP73 microscope. Quantification analysis of the numbers of infiltrated leukocytes ($CD45^+$) and macrophages ($Mac2^+$) in the aortic wall and the expression of MMP9 in the endothelium were performed with Image J software.

Dihydroethidium staining

The Dihydroethidium (DHE) staining of mouse aorta sections and HAECs was conducted as previously described (54). Briefly, the suprarenal abdominal aortas (AngII-induced AAA) and infrarenal abdominal aortas (elastase-induced AAA) were embedded in OCT. Serial cryosections (7 μm thick, 200 μm apart) were rehydrated in PBS (pH 7.5). The aorta sections were immediately incubated with fresh DHE staining solution (dissolved in PBS at a concentration of 5 μM) for 30min at 37°C protected from light. After washing three times with PBS, the slides were mounted with ProLong™ Gold Antifade Mountant with DAPI (Invitrogen, P36935), and images were captured with an Olympus DP73 microscope. Quantitative analysis of the DHE fluorescence within the aortic wall was performed with Image J software.

HAECs were transfected with siControl, si*KLF11*, si*KLF11*+si*NOX2* for 48h, or treated with *NOX2* inhibitor for 1h, and then stimulated with TNF-α (2 ng/ml) or AngII (1μM) for 2h or their corresponding vehicle controls. Next, the cells were subjected to DHE staining, image collection and quantification analysis of the DHE fluorescence in the HAECs were performed as described above.

Bone marrow transplantation

The protocol for syngeneic bone marrow transplantation (BMT) was performed as previously described (20, 21). In brief, the recipient mice at 6-week of age were given 13 Gy (1300 rad) whole-body irradiation from a 137 Cesium Gamma source. The donor bone marrow cells were isolated from the femurs of WT mice and resuspended at a concentration of $2x10^7$ cells/ml in serum-free RPMI (RPMI 1640 + 20 mM HEPES+50 mg/ml of a penicillin/streptomycin solution). A mixture of $5x10^6$ bone marrow cells (total volume = 250 μl) was injected by tail vein into each of the recipient mice 4 hours after irradiation. Two weeks after BMT, the elastase-induced AAA model was performed on the recipient mice.

Apoptosis assay

The DeadEnd™ Fluorometric TUNEL (terminal deoxynucleotidyl transferase dUTP nick-end labeling) system (Promega, G3250, Madison, WI) was used to detect the vascular cell apoptosis within the aortic wall according to the manufacturer's protocol. Briefly, the sectioned aortic tissue (7 μm thick) was permeabilized with Proteinase K solution (20μg/ml) for 10 min at room temperature, and then incubated with equilibration buffer for 10 min at room temperature. The TdT (terminal deoxynucleotidyl transferase) reaction mixture was added to the aortic tissues for 60 min with incubation at 37°C, followed by 2xSSC buffer to stop the reaction. Slides were mounted with ProLong™ Gold Antifade Mountant with DAPI (Invitrogen, P36935), and the green fluorescence of apoptotic cells within the aortic wall was captured with an Olympus DP73 microscope.

The ApopTag Peroxidase in Situ Apoptosis Detection Kit (Millipore Sigma, S7100) was used to detect the apoptosis of cultured HAECs according to the manufacturer's instructions. Briefly, HAECs were fixed in 1% paraformaldehyde for 10 min at room temperature and a precooled mixture of ethanol and acetic acid (2:1 by volume) for 5 min at -20°C sequentially, followed by 3% hydrogen peroxide for 5 min at room temperature to quench endogenous peroxidase. After incubation in equilibration buffer, HAECs were treated with working strength TdT enzyme solution for 60 min at 37°C, followed by working strength Stop/Wash buffer to stop the reaction. Then anti-digoxigenin conjugate and peroxidase substrate were sequentially incubated with HAECs, and the apoptotic cells were recorded by microscopy.

siRNA Transfection

HAECs were transfected with 30 nM si*KLF11*(ThermoFisher Scientific, s13158), si*NOX2* (ThermoFisher Scientific, s531915), or Silencer™ Select Negative Control siRNA (siControl, ThermoFisher Scientific, 4390843) using Lipofectamine RNAiMAX Reagent (Invitrogen, 13778150) according to the manufacturer's instructions.

Total RNA Isolation and Quantitative Real-time PCR Analysis

Total RNA from HAECs or HASMCs was extracted using RNeasy Mini Kit (QIAGEN, 74106, Hilden, Germany) according to the manufacturer's instructions. SuperScript™ III First-Strand Synthesis System (Thermo Fisher Scientific, 18080051) and random primers were used to reverse transcribe RNA into cDNA. Gene expression was quantified by Real-Time PCR Detection System (BioRad, Hercules, CA) using iQ SYBR Green Supermix (1708882, Bio-Rad, Hercules, CA). The gene expression level was normalized to the internal control GAPDH. The primer sequences used are listed in Supplementary Table 6.

RNA-sequencing

Total RNA was extracted from HACECs 48h after infection with Ad-sh*lacZ* (n=3) or Ad-sh*KLF11* (n=4), using RNeasy Mini Kit (QIAGEN, 74106, Hilden, Germany) and then treated with RNAase-free DNase I (QIAGEN, 79254) according to the manufacturer's instructions. RNA library preparation and sequencing were performed by the Advanced Genomics Core at the University of Michigan. In brief, RNA quality was determined by BioAnalyzer (Agilent) before sequencing. The RNA library was prepared with NEBNext Ultra RNA Library Prep Kit (New England Biolabs, Ipswich, MA) and 51bp reads paired-end sequencing was performed on a HiSeq 6000 platform (Illumina). A total of 266 million reads were generated, with an average of 38 million reads for each sample. RNAseq read mapping was performed as described previously (55). Briefly, FastQC (Babraham Bioinformatics) was used for quality control of the sequencing reads from each sample. Gene expression quantification was performed using Salmon v 0.14.0 (56), with human cDNA sequences of GRCh38 (Ensembl database) as reference. The differential expression analysis was performed with the DeSeq2 package in R (57). Gene Set Enrichment Analysis (GSEA) (58, 59) was performed to interpret gene expression profiles of Ad-sh*lacZ* and Ad-sh*KLF11* infected HAECs. Genes were mapped to the HALLMARK and GO gene set in the Molecular Signatures Database (MSigDB) for pathway

analysis. The RNA-seq raw data and processed data described in the paper has been deposited in the Gene Expression Omnibus database (https://www.ncbi.nlm.nih.gov/geo/) under the accession code GSE152468.

Protein extraction and Western blot

Cells were lysed in RIPA lysis buffer (Thermo Fisher Scientific, 89901, Waltham, MA) supplemented with the cOmplete™ EDTA-free protease inhibitor cocktail (Roche, 11873580001, Penzberg, Germany) and PhosSTOP™ phosphatase inhibitor (Roche, 4906845001, Penzberg, Germany). Protein extracts were resolved in 10% SDS-PAGE gels and transferred to nitrocellulose membranes (BioRad, 1620115, Hercules, CA). Membranes were blocked in TBST containing 5% fat-free milk for 1 hour at room temperature and incubated with primary antibodies at 4 °C overnight. After washing three times with 1xTBST, membranes were incubated with secondary antibody (1:10,000 dilution, Li-Cor Bioscience, Lincoln, NE) for 1 hour at room temperature. After three washes with 1xTBST, bands were scanned using Odyssey Imaging System (Li-Cor Bioscience, Lincoln, NE) and quantified with the LI-COR Image Studio Software.

Leukocyte-endothelial adhesion assay

The THP-1 and HAECs adhesion assay was performed as described before (14). In brief, THP-1 cells were infected with Ad-*GFP*. HAECs were infected with Ad-*lacZ*, Ad-*KLF11*, or transfected with siControl, si*KLF11*. After 48h, HAECs were treated with TNF-α (2 ng/ml) or vehicle control for 4h and subsequently incubated for 30 min with Ad-*GFP*-infected THP-1 cells. The unbound THP-1 cells were removed by washing with PBS three times. The adhered cells were fixed with 4% paraformaldehyde, photographed by fluorescence microscopy and numbers were calculated from 9 random fields per well using Image J software.

Endothelial cell conditioned media (EC-CM) and Gelatin Zymography

A total of $2x10^4/cm^2$ HAECs seeded in 6-well culture plates in 10% serum containing medium were infected with Ad-*GFP*, Ad-*KLF11*, Ad-sh*lacZ* or Ad-sh*KLF11* (10 MOI). After 48h, HAECs were treated with human recombinant TNF-α (2 ng/ml) for 1h, and then cultured in fresh opti-MEM medium. After 4h, media were collected as endothelial cell-conditioned medium (EC-CM) and transferred to HASMCs for 24h.

Gelatin zymography was performed as previously described (51). Briefly, equal volumes of EC-CM were electrophoresed on SDS-PAGE gels containing 1 mg/ml gelatin (Millipore Sigma, G8150). Gels were washed three times in 2.5% Triton X-100 and incubated in zymography buffer (50 mM Tris-HCl, 150 mM NaCl, 10 mM $CaCl_2$, and 0.05% sodium azide) for 48 hours at 37°C. Gels were stained/destained with eStain L1 Protein Staining kit (Genscript, M00549) using the eStain L1 Protein Staining Device (Genscript).

Chromatin Immunoprecipitation (ChIP) assay

ChIP assays were performed using the SimpleChIP Enzymatic Chromatin IP kit (Magnetic Beads) (CST, 9003S) according to the manufacturer's protocol. In brief, HAECs were infected with Ad-*lacZ* or Ad-flag-*KLF11*. After 48h, HAECs were incubated with 1% formaldehyde for 10 min at room temperature, and the cross-linking was stopped by 0.1% glycine at room temperature for 5 min. The nuclei pellets were digested with Micrococcal Nuclease at 37°C for 20 min, followed by sonication (Branson Sonifier SLPe, 10 seconds of 35% amplification, three times). After centrifugation, the chromatin was incubated with an anti-flag antibody (1:100, CST, 14793S) or normal rabbit IgG (CST, 2729) at 4°C overnight with gentle rotation. The DNA/protein complexes were immunoprecipitated by ChIP grade protein G magnetic beads with rotation for 2 hours at 4°C, followed by three wash in low-salt buffer and one wash in high-salt buffer, and elution at 65°C for 30 min. The eluted DNA-protein complexes were reversed with

proteinase K at 65°C for 2 hours. The DNA was purified and then amplified by real-time quantitative PCR with the following primers targeted to the Mmp9 promoter (-626/-535), forward primer: 5'-AGTGGAATTCCCCAGCCTT-3' and reverse primer: 5'-CCTGACAGCCTTCTTTGACTCA-3'. Nox2 promoter (-720/-620), forward primer: 5'-TCAAAGTGCTGGGATTACAGGC-3' and reverse primer: 5'-GCTTTGGCCAATGATGATGAACCAC-3'.

Cellular ROS/Superoxide Detection Assay

The production of superoxide and ROS in HAECs was measured using the Cellular ROS/Superoxide Detection Assay Kit (Abcam, ab139476) following the manufacturer's protocol. Briefly, HAECs were infected with Ad-sh*KLF11*, Ad-*KLF11* or transfected with si*KLF11*, si*NOX2* and after 48h, seeded in 96 well black wall/clear bottom plates at a density of $1.5x10^4$ cells/wall. Negative control samples were pre-treated with a ROS inhibitor (N-acetyl-L-cysteine) 30 minutes prior to stimulation. HAECs were stimulated with TNF-α (2 ng/ml) or AngII (1 μM) and 100 μl/well of ROS/Superoxide detection solution was simultaneously added to cells for 2h at 37°C in the dark. The fluorescence was detected using a fluorescence microplate reader at Ex/Em=490/520 nm (for ROS) and Ex/Em= 520/600 nm (for Superoxide).

Statistical Analysis

Statistical analyses were performed using GraphPad Prism 8.0 software (GraphPad Software, San Diego, CA) or RStudio (for RNA-seq). Unless indicated otherwise, data are presented as mean ± standard error of the mean (SEM). All data were evaluated for normality and variance. For normally distributed data, Student's *t*-test was used to compare the difference between two groups, and one-way ANOVA followed by Tukey's post hoc analysis or two-way ANOVA followed by Holm-Sidak post hoc analysis were used for comparison among three or more groups. For data that were not normally distributed, non-parametric tests including Mann-

Whitney test, Chi-squared test or Mantel-Cox test (survival percentage) were used to compare two groups. *P* value < 0.05 was considered as statistically significant. All results are representative of at least 3 independent experiments.

Study Approval

All animal studies and experimental procedures were performed according to the protocols approved by the Institutional Animal Care & Use Committee (IACUC) at the University of Michigan. The human samples used in this study were obtained from the Cardiovascular Health Improvement Project (CHIP) core in the Department of Cardiac Surgery at the University of Michigan with the Institutional Review Board approval (Hum0077616) from the Human Research Protection Program and Institutional Review Boards of the University of Michigan Medical School.

Author Contributions: G. Zhao, Z. Chang, Y. Zhao, and J. Zhang performed the experiments and results analysis. G. Zhao and J. Zhang wrote the article. Y. Guo, H. Lu, W. Liang, O. Rom, J. Sun, H. Wang, T. Zhu, Y. Fan, L. Chang, B. Yan, M.T. Garcia-Barrio provided technical support and contributed to the discussion of the project. M.T. Garcia-Barrio did the critical editing of the article. Y.E. Chen and J. Zhang designed the research and discussed the results.

Acknowledgments

This study was partially supported by National Institutes of Health grants HL138139 (J. Zhang), HL068878 and HL134569 (Y.E. Chen), HL122664 (L. Chang), HL145176 (Y. Fan), HL150233 (O. Rom), American Heart Association grants 20P0ST35110064 (G. Zhao) and 18PRE34000005 (W. Liang).

References

1. Golledge J, Muller J, Daugherty A, and Norman P. Abdominal aortic aneurysm: pathogenesis and implications for management. *Arterioscler Thromb Vasc Biol.* 2006;26(12):2605-13.
2. Davis FM, Daugherty A, and Lu HS. Updates of Recent Aortic Aneurysm Research. *Arterioscler Thromb Vasc Biol.* 2019;39(3):e83-e90.
3. Golledge J. Abdominal aortic aneurysm: update on pathogenesis and medical treatments. *Nature Reviews Cardiology.* 2019;16(4):225-42.
4. Godo S, and Shimokawa H. Endothelial Functions. *Arterioscler Thromb Vasc Biol.* 2017;37(9):e108-e14.
5. Gimbrone MA, Jr., and García-Cardeña G. Endothelial Cell Dysfunction and the Pathobiology of Atherosclerosis. *Circ Res.* 2016;118(4):620-36.
6. Cheng D, Talib J, Stanley CP, Rashid I, Michaelsson E, Lindstedt EL, et al. Inhibition of MPO (Myeloperoxidase) Attenuates Endothelial Dysfunction in Mouse Models of Vascular Inflammation and Atherosclerosis. *Arterioscler Thromb Vasc Biol.* 2019;39(7):1448-57.
7. Higashi Y, Noma K, Yoshizumi M, and Kihara Y. Endothelial Function and Oxidative Stress in Cardiovascular Diseases. *Circulation Journal.* 2009;73(3):411-8.
8. Ramella M, Boccafoschi F, Bellofatto K, Follenzi A, Fusaro L, Boldorini R, et al. Endothelial MMP-9 drives the inflammatory response in abdominal aortic aneurysm (AAA). *Am J Transl Res.* 2017;9(12):5485-95.
9. Saito T, Hasegawa Y, Ishigaki Y, Yamada T, Gao J, Imai J, et al. Importance of endothelial NF-κB signalling in vascular remodelling and aortic aneurysm formation. *Cardiovascular Research.* 2012;97(1):106-14.
10. Franck G, Dai J, Fifre A, Ngo S, Justine C, Michineau S, et al. Reestablishment of the endothelial lining by endothelial cell therapy stabilizes experimental abdominal aortic aneurysms. *Circulation.* 2013;127(18):1877-87.
11. Sun J, Deng H, Zhou Z, Xiong X, and Gao L. Endothelium as a Potential Target for Treatment of Abdominal Aortic Aneurysm. *Oxid Med Cell Longev.* 2018;2018:6306542.
12. Fan Y, Lu H, Liang W, Hu W, Zhang J, and Chen YE. Krüppel-like factors and vascular wall homeostasis. *Journal of Molecular Cell Biology.* 2017;9(5):352-63.
13. Suzuki T, Aizawa K, Matsumura T, and Nagai R. Vascular Implications of the Krüppel-Like Family of Transcription Factors. *Arteriosclerosis, Thrombosis, and Vascular Biology.* 2005;25(6):1135-41.
14. Fan Y, Guo Y, Zhang J, Subramaniam M, Song C-Z, Urrutia R, et al. Krüppel-like factor-11, a transcription factor involved in diabetes mellitus, suppresses endothelial cell activation via the nuclear factor-κB signaling pathway. *Arteriosclerosis, thrombosis, and vascular biology.* 2012;32(12):2981-8.
15. Liang W, Fan Y, Lu H, Chang Z, Hu W, Sun J, et al. KLF11 (Kruppel-Like Factor 11) Inhibits Arterial Thrombosis via Suppression of Tissue Factor in the Vascular Wall. *Arterioscler Thromb Vasc Biol.* 2019;39(3):402-12.
16. Yin K-J, Fan Y, Hamblin M, Zhang J, Zhu T, Li S, et al. KLF11 mediates PPARγ cerebrovascular protection in ischaemic stroke. *Brain.* 2013;136(Pt 4):1274-87.
17. Bhamidipati CM, Mehta GS, Lu G, Moehle CW, Barbery C, DiMusto PD, et al. Development of a novel murine model of aortic aneurysms using peri-adventitial elastase. *Surgery.* 2012;152(2):238-46.
18. Lu H, Howatt DA, Balakrishnan A, Graham MJ, Mullick AE, and Daugherty A. Hypercholesterolemia Induced by a PCSK9 Gain-of-Function Mutation Augments Angiotensin II-Induced Abdominal Aortic Aneurysms in C57BL/6 Mice-Brief Report. *Arteriosclerosis, thrombosis, and vascular biology.* 2016;36(9):1753-7.

19. Lu H, Sun J, Liang W, Chang Z, Rom O, Zhao Y, et al. Cyclodextrin Prevents Abdominal Aortic Aneurysm via Activation of Vascular Smooth Muscle Cell Transcription Factor EB. *Circulation.* 2020;142(5):483-98.
20. Tilley Rachel E, Pedersen B, Pawlinski R, Sato Y, Erlich Jonathan H, Shen Y, et al. Atherosclerosis in Mice Is Not Affected by a Reduction in Tissue Factor Expression. *Arteriosclerosis, Thrombosis, and Vascular Biology.* 2006;26(3):555-62.
21. Bodary PF, Westrick RJ, Wickenheiser KJ, Shen Y, and Eitzman DT. Effect of Leptin on Arterial Thrombosis Following Vascular Injury in Mice. *JAMA.* 2002;287(13):1706-9.
22. Rabkin SW. The Role Matrix Metalloproteinases in the Production of Aortic Aneurysm. *Prog Mol Biol Transl Sci.* 2017;147:239-65.
23. Pyo R, Lee JK, Shipley JM, Curci JA, Mao D, Ziporin SJ, et al. Targeted gene disruption of matrix metalloproteinase-9 (gelatinase B) suppresses development of experimental abdominal aortic aneurysms. *The Journal of Clinical Investigation.* 2000;105(11):1641-9.
24. Chase Alexander J, Bond M, Crook Martin F, and Newby Andrew C. Role of Nuclear Factor-κB Activation in Metalloproteinase-1, -3, and -9 Secretion by Human Macrophages In Vitro and Rabbit Foam Cells Produced In Vivo. *Arteriosclerosis, Thrombosis, and Vascular Biology.* 2002;22(5):765-71.
25. Tacon CE, Wiehler S, Holden NS, Newton R, Proud D, and Leigh R. Human rhinovirus infection up-regulates MMP-9 production in airway epithelial cells via NF-{kappa}B. *Am J Respir Cell Mol Biol.* 2010;43(2):201-9.
26. McCormick Michael L, Gavrila D, and Weintraub Neal L. Role of Oxidative Stress in the Pathogenesis of Abdominal Aortic Aneurysms. *Arteriosclerosis, Thrombosis, and Vascular Biology.* 2007;27(3):461-9.
27. Miller Francis J, Sharp William J, Fang X, Oberley Larry W, Oberley Terry D, and Weintraub Neal L. Oxidative Stress in Human Abdominal Aortic Aneurysms. *Arteriosclerosis, Thrombosis, and Vascular Biology.* 2002;22(4):560-5.
28. Fan LM, Douglas G, Bendall JK, McNeill E, Crabtree MJ, Hale AB, et al. Endothelial cell-specific reactive oxygen species production increases susceptibility to aortic dissection. *Circulation.* 2014;129(25):2661-72.
29. Nanami M, Ookawara T, Otaki Y, Ito K, Moriguchi R, Miyagawa K, et al. Tumor necrosis factor-alpha-induced iron sequestration and oxidative stress in human endothelial cells. *Arterioscler Thromb Vasc Biol.* 2005;25(12):2495-501.
30. Guzik TJ, West Ne Fau - Black E, Black E Fau - McDonald D, McDonald D Fau - Ratnatunga C, Ratnatunga C Fau - Pillai R, Pillai R Fau - Channon KM, et al. Vascular superoxide production by NAD(P)H oxidase: association with endothelial dysfunction and clinical risk factors. (1524-4571 (Electronic)).
31. Schramm A, Matusik P Fau - Osmenda G, Osmenda G Fau - Guzik TJ, and Guzik TJ. Targeting NADPH oxidases in vascular pharmacology. (1879-3649 (Electronic)).
32. Meza CA, La Favor JD, Kim DH, and Hickner RC. Endothelial Dysfunction: Is There a Hyperglycemia-Induced Imbalance of NOX and NOS? *Int J Mol Sci.* 2019;20(15).
33. Shimizu K, Mitchell RN, and Libby P. Inflammation and cellular immune responses in abdominal aortic aneurysms. *Arterioscler Thromb Vasc Biol.* 2006;26(5):987-94.
34. Sattar N. Inflammation and endothelial dysfunction: intimate companions in the pathogenesis of vascular disease? *Clin Sci (Lond).* 2004;106(5):443-5.
35. Zhang H, Park Y, Wu J, Chen X, Lee S, Yang J, et al. Role of TNF-alpha in vascular dysfunction. *Clin Sci (Lond).* 2009;116(3):219-30.
36. Qin Y, Cao X, Yang Y, and Shi GP. Cysteine protease cathepsins and matrix metalloproteinases in the development of abdominal aortic aneurysms. *Future Cardiol.* 2013;9(1):89-103.

37. Vorkapic E, Folkesson M, Magnell K, Bohlooly-Y M, Länne T, and Wågsäter D. ADAMTS-1 in abdominal aortic aneurysm. *PLOS ONE.* 2017;12(6):e0178729.
38. Sun J, Sukhova GK, Zhang J, Chen H, Sjoberg S, Libby P, et al. Cathepsin K deficiency reduces elastase perfusion-induced abdominal aortic aneurysms in mice. *Arterioscler Thromb Vasc Biol.* 2012;32(1):15-23.
39. Adair-Kirk TL, and Senior RM. Fragments of extracellular matrix as mediators of inflammation. *Int J Biochem Cell Biol.* 2008;40(6):1101-10.
40. Sorokin L. The impact of the extracellular matrix on inflammation. *Nature Reviews Immunology.* 2010;10(10):712-23.
41. Gaggar A, Jackson PL, Noerager BD, O'Reilly PJ, McQuaid DB, Rowe SM, et al. A Novel Proteolytic Cascade Generates an Extracellular Matrix-Derived Chemoattractant in Chronic Neutrophilic Inflammation. *The Journal of Immunology.* 2008;180(8):5662.
42. Incalza MA, D'Oria R, Natalicchio A, Perrini S, Laviola L, and Giorgino F. Oxidative stress and reactive oxygen species in endothelial dysfunction associated with cardiovascular and metabolic diseases. *Vascular Pharmacology.* 2018;100:1-19.
43. Zhang Y, Murugesan P, Huang K, and Cai H. NADPH oxidases and oxidase crosstalk in cardiovascular diseases: novel therapeutic targets. *Nature Reviews Cardiology.* 2020;17(3):170-94.
44. Mittal M, Siddiqui MR, Tran K, Reddy SP, and Malik AB. Reactive oxygen species in inflammation and tissue injury. *Antioxid Redox Signal.* 2014;20(7):1126-67.
45. Cafueri G, Parodi F, Pistorio A, Bertolotto M, Ventura F, Gambini C, et al. Endothelial and smooth muscle cells from abdominal aortic aneurysm have increased oxidative stress and telomere attrition. *PLoS One.* 2012;7(4):e35312.
46. Li J-M, Fan LM, Christie MR, and Shah AM. Acute tumor necrosis factor alpha signaling via NADPH oxidase in microvascular endothelial cells: role of p47phox phosphorylation and binding to TRAF4. *Mol Cell Biol.* 2005;25(6):2320-30.
47. Gavrila D, Li WG, McCormick ML, Thomas M, Daugherty A, Cassis LA, et al. Vitamin E inhibits abdominal aortic aneurysm formation in angiotensin II-infused apolipoprotein E-deficient mice. *Arteriosclerosis, thrombosis, and vascular biology.* 2005;25(8):1671-7.
48. Hergenreider E, Heydt S, Tréguer K, Boettger T, Horrevoets AJG, Zeiher AM, et al. Atheroprotective communication between endothelial cells and smooth muscle cells through miRNAs. *Nature Cell Biology.* 2012;14(3):249-56.
49. Gao Y, Chen T, and Raj JU. Endothelial and Smooth Muscle Cell Interactions in the Pathobiology of Pulmonary Hypertension. *Am J Respir Cell Mol Biol.* 2016;54(4):451-60.
50. He L, Fu Y, Deng J, Shen Y, Wang Y, Yu F, et al. Deficiency of FAM3D (Family With Sequence Similarity 3, Member D), A Novel Chemokine, Attenuates Neutrophil Recruitment and Ameliorates Abdominal Aortic Aneurysm Development. *Arterioscler Thromb Vasc Biol.* 2018;38(7):1616-31.
51. Zhao G, Fu Y, Cai Z, Yu F, Gong Z, Dai R, et al. Unspliced XBP1 Confers VSMC Homeostasis and Prevents Aortic Aneurysm Formation via FoxO4 Interaction. *Circ Res.* 2017;121(12):1331-45.
52. Sobczak M, Dargatz J, and Chrzanowska-Wodnicka M. Isolation and culture of pulmonary endothelial cells from neonatal mice. *J Vis Exp.* 2010(46).
53. Hu W, Lu H, Zhang J, Fan Y, Chang Z, Liang W, et al. Krüppel-like factor 14, a coronary artery disease associated transcription factor, inhibits endothelial inflammation via NF-κB signaling pathway. *Atherosclerosis.* 2018;278:39-48.
54. Wang Q, and Zou M-H. In: Neumann D, and Viollet B eds. *AMPK: Methods and Protocols*. New York, NY: Springer New York; 2018:507-17.

55. Lu H, Sun J, Liang W, Zhang J, Rom O, Garcia-Barrio MT, et al. Novel gene regulatory networks identified in response to nitro-conjugated linoleic acid in human endothelial cells. *Physiological Genomics.* 2019;51(6):224-33.
56. Patro R, Duggal G, Love MI, Irizarry RA, and Kingsford C. Salmon provides fast and bias-aware quantification of transcript expression. *Nature Methods.* 2017;14(4):417-9.
57. Love MI, Huber W, and Anders S. Moderated estimation of fold change and dispersion for RNA-seq data with DESeq2. *Genome Biology.* 2014;15(12):550.
58. Subramanian A, Tamayo P, Mootha VK, Mukherjee S, Ebert BL, Gillette MA, et al. Gene set enrichment analysis: a knowledge-based approach for interpreting genome-wide expression profiles. *Proceedings of the National Academy of Sciences of the United States of America.* 2005;102(43):15545-50.
59. Reimand J, Isserlin R, Voisin V, Kucera M, Tannus-Lopes C, Rostamianfar A, et al. Pathway enrichment analysis and visualization of omics data using g:Profiler, GSEA, Cytoscape and EnrichmentMap. *Nature Protocols.* 2019;14(2):482-517.

Figures

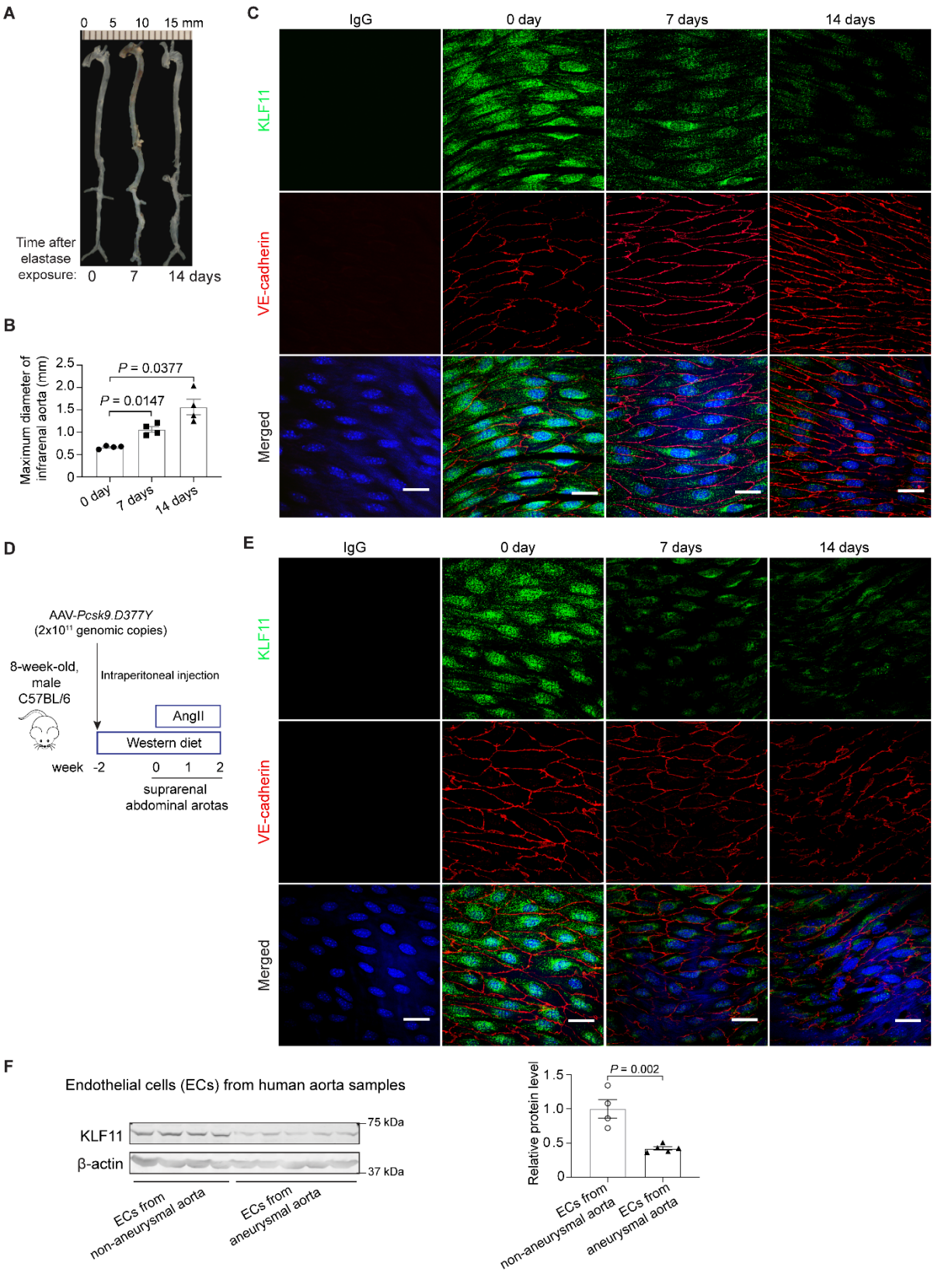
A
0 5 10 15 mm
Time after elastase exposure: 0 7 14 days
B
Maximum diameter of infrarenal aorta (mm)
P = 0.0377
P = 0.0147
0 day
7 days
14 days
C
IgG
0 day
7 days
14 days
KLF11
VE-cadherin
Merged
D
AAV-Pcsk9.D377Y
(2x10^11 genomic copies)
8-week-old, male C57BL/6
Intraperitoneal injection
AngII
Western diet
week -2 0 1 2
suprarenal abdominal arotas
E
IgG
0 day
7 days
14 days
KLF11
VE-cadherin
Merged
F
Endothelial cells (ECs) from human aorta samples
KLF11
β-actin
75 kDa
37 kDa
ECs from non-aneurysmal aorta
ECs from aneurysmal aorta
Relative protein level
P = 0.002
ECs from non-aneurysmal aorta
ECs from aneurysmal aorta

1

Figure 1. KLF11 is reduced in the endothelial cells of mouse and human aortic aneurysms. A-C. Elastase-induced AAA model in 10-week-old C57BL/6 male mice (n=4/group). Representative morphology of aortas (**A**) and quantification of maximal infrarenal aortic diameters (**B**). *En face* immunofluorescence staining of KLF11 (green) and VE-cadherin (red, EC marker) in the endothelium of elastase-treated infrarenal aortas (**C**) and AngII-infused suprarenal abdominal aortas (**D-E**) from the indicated end-time points. Nuclei stained by DAPI are blue. Scale bar=20μm. **F**, Western blot analysis of KLF11 expression in the endothelial cells from human normal (n=4) and aneurysmal aortas (n=5). Data are presented as mean±SEM. One-way ANOVA followed by Tukey's post hoc for B, Student's *t*-test for E.

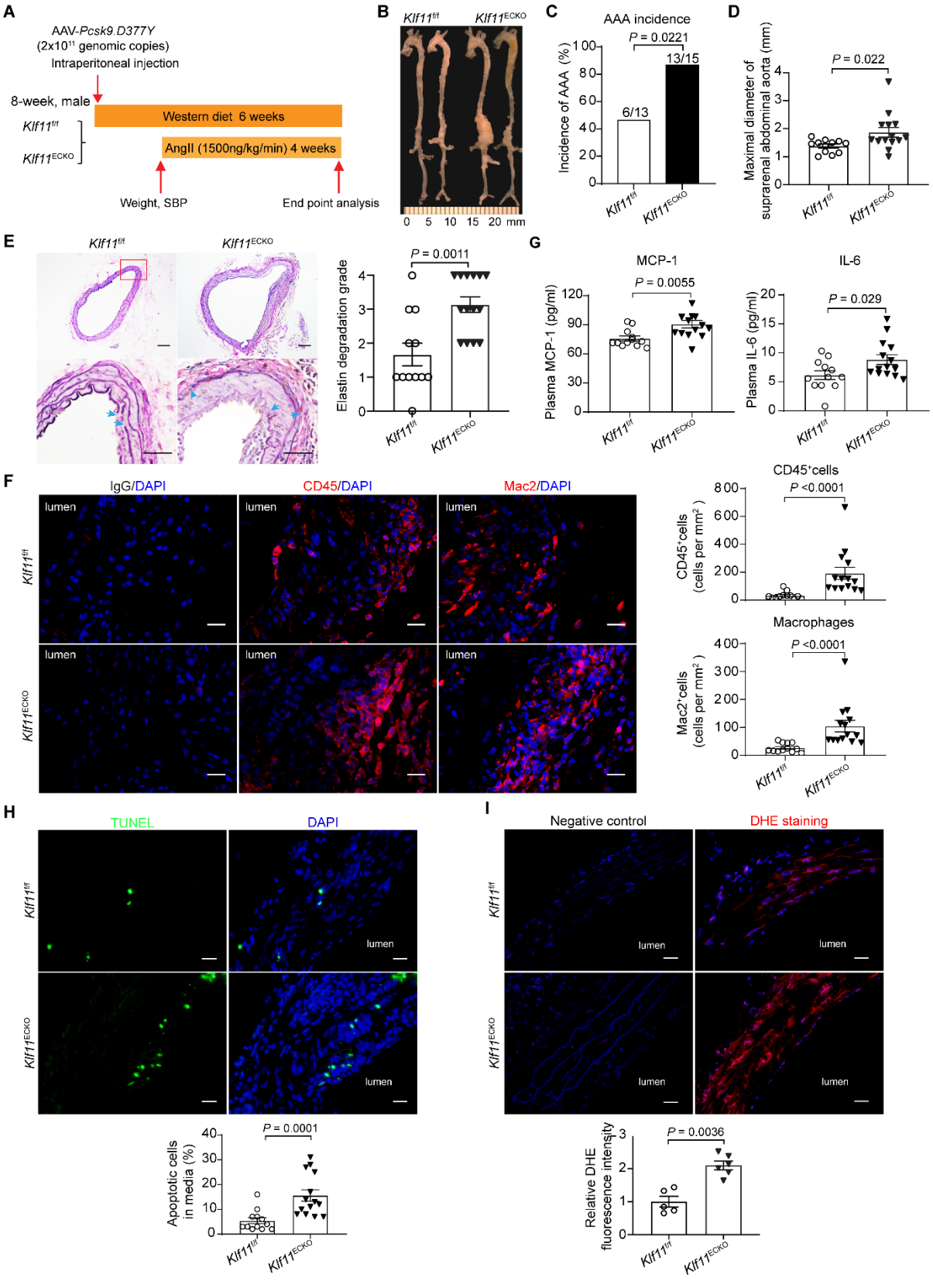
A
AAV-Pcsk9.D377Y
(2x10^11 genomic copies)
Intraperitoneal injection
8-week, male
Klf11f/f
Klf11ECKO
Western diet 6 weeks
AngII (1500ng/kg/min) 4 weeks
Weight, SBP
End point analysis
B
Klf11f/f
Klf11ECKO
0 5 10 15 20 mm
C
AAA incidence
P = 0.0221
13/15
6/13
Incidence of AAA (%)
D
P = 0.022
Maximal diameter of suprarenal abdominal aorta (mm)
E
Klf11f/f
Klf11ECKO
P = 0.0011
Elastin degradation grade
G
MCP-1
P = 0.0055
Plasma MCP-1 (pg/ml)
IL-6
P = 0.029
Plasma IL-6 (pg/ml)
F
IgG/DAPI
CD45/DAPI
Mac2/DAPI
lumen
CD45+cells
P <0.0001
CD45+cells (cells per mm2)
Macrophages
P <0.0001
Mac2+cells (cells per mm2)
H
TUNEL
DAPI
P = 0.0001
Apoptotic cells in media (%)
I
Negative control
DHE staining
P = 0.0036
Relative DHE fluorescence intensity

1

Figure 2. Endothelial cell-specific KLF11 depletion aggravates *Pcsk9*/AngII-induced AAA. The *Pcsk9*/AngII-induced AAA model was performed on 8-week-old male with EC-specific *Klf11* knockout (*Klf11*^{ECKO}, n=15) and their littermate floxed-*Klf11* (*Klf11*$^{f/f}$, n=13) mice. **A**. Schematics of *Pcsk9*/AngII-induced AAA model. **B**. Representative morphology of aortas from AngII-infused *Klf11*$^{f/f}$ and *Klf11*^{ECKO} mice. **C**. Incidence of AAA. **D**. Maximal diameters of suprarenal abdominal aortas (SAAs) from AngII-infused *Klf11*$^{f/f}$ (n=12) and *Klf11*^{ECKO} (n=14) mice. **E**. Representative Verhoeff-Van Gieson (VVG) staining and quantification of elastin degradation in SAAs from AngII-infused *Klf11*$^{f/f}$ (n=12) and *Klf11*^{ECKO} (n=14) mice. Scale bar=50μm. **F**. Representative immunofluorescence staining and quantification of leukocyte ($CD45^+$) and macrophage ($Mac2^+$) infiltration in the aortic wall of SAAs from AngII-infused *Klf11*$^{f/f}$ (n=12) and *Klf11*^{ECKO} (n=14) mice. Scale bar=20μm. **G**. ELISA analysis of MCP-1 and IL-6 in the plasma from AngII-infused *Klf11*$^{f/f}$ (n=12) and *Klf11*^{ECKO} (n=14) mice. **H**. Representative TUNEL staining (green) and quantification of apoptotic cells in the media of SAAs from AngII-infused *Klf11*$^{f/f}$ (n=12) and *Klf11*^{ECKO} (n=14) mice. Scale bar=20μm. **I**. Representative DHE staining (red) and quantification of ROS production in the aortic wall of SAAs from AngII-infused *Klf11*$^{f/f}$ (n=5) and *Klf11*^{ECKO} (n=6). Scale bar=20μm. Data are presented as mean±SEM. Chi-square test for C, Student's *t*-test for D, G and I, Mann-Whitney test for E-F, H.

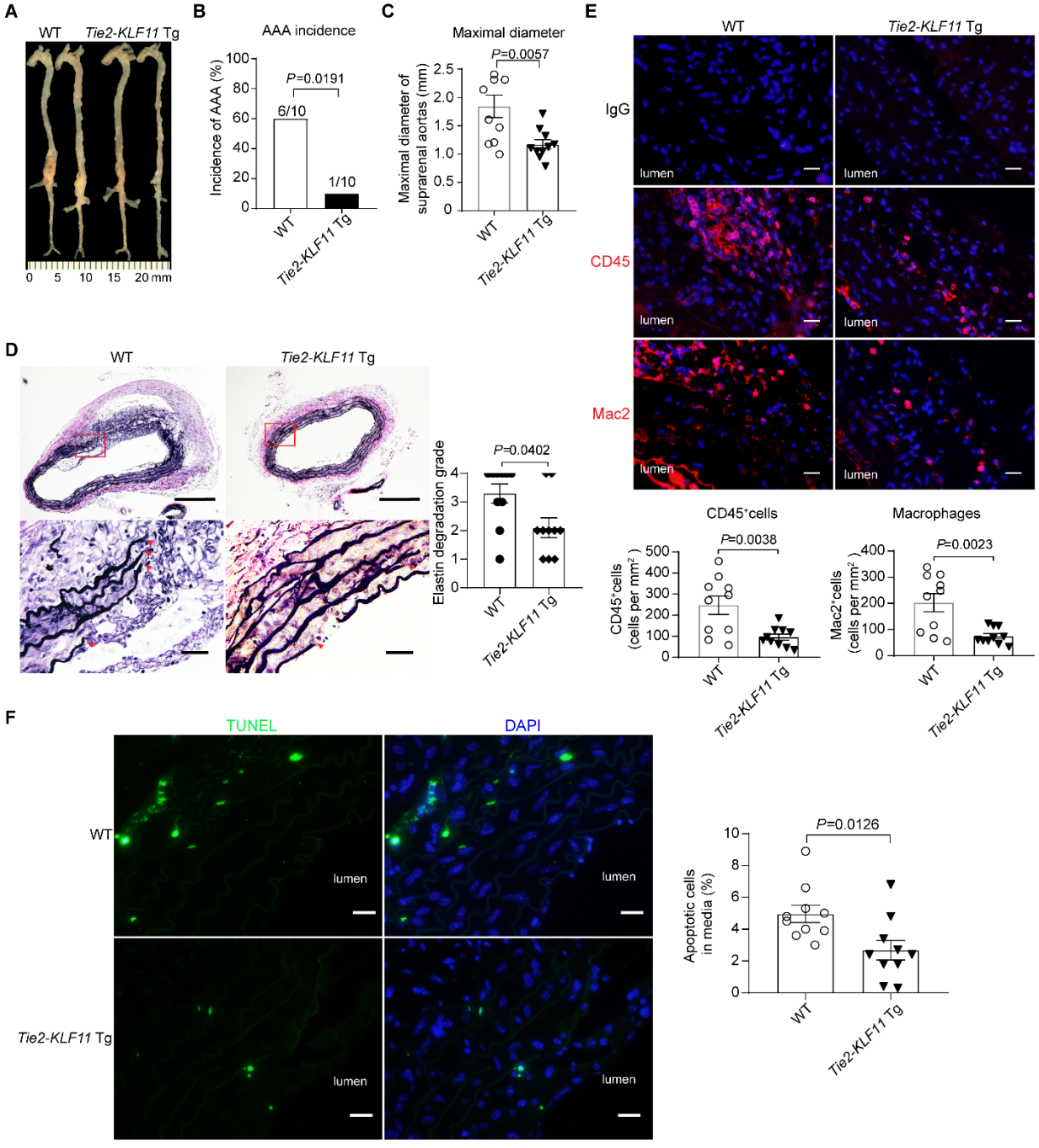

Figure 3. Endothelial cell-selective overexpression of KLF11 attenuates *Pcsk9*/AngII-induced AAA. The *Pcsk9*/AngII-induced AAA model was performed on 10-week-old male EC-selective *KLF11* transgenic mice (*Tie2-KLF11* Tg, n=12) and littermate control mice (WT, n=13). **A**. Representative morphology of aortas from AngII-infused WT and *Tie2-KLF11* Tg mice. **B**. Incidence of AAA. **C**. Maximal diameters of SAAs. **D**. Representative VVG staining and

quantification of elastin degradation in SAAs from WT and *Tie2-KLF11* Tg mice (n=10/group). Scale bar=200 μm for whole aortic sections; scale bar=20 μm for magnified areas. **E**. Representative immunofluorescence staining and quantification of leukocyte ($CD45^+$) and macrophage ($Mac2^+$) infiltration in the aortic wall of SAAs from WT and *Tie2-KLF11* Tg mice (n=10/group). Scale bar=20μm. **F**. Representative TUNEL staining (green) and quantification of apoptotic cells in the media of SAAs from WT and *Tie2-KLF11* Tg mice (n=10/group). Scale bar=20μm. Data are presented as mean±SEM. Chi-square test for B, Student's *t*-test for C and E-F, Mann-Whitney test for D.

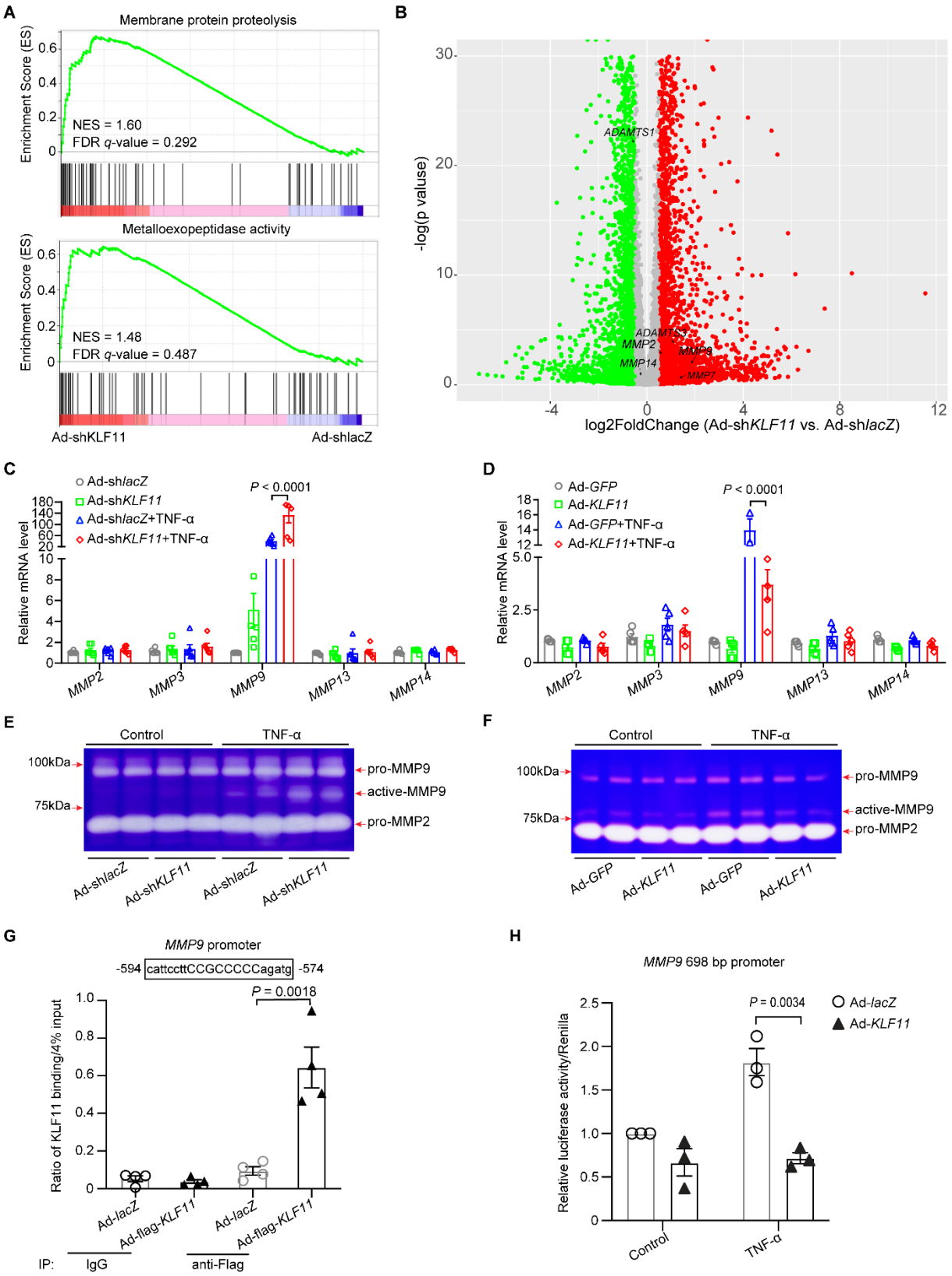
A
Membrane protein proteolysis
Enrichment Score (ES)
NES = 1.60
FDR q-value = 0.292
Metalloexopeptidase activity
NES = 1.48
FDR q-value = 0.487
Ad-shKLF11
Ad-shlacZ
B
-log(p value)
log2FoldChange (Ad-shKLF11 vs. Ad-shlacZ)
ADAMTS1
ADAMTS4
MMP2
MMP9
MMP14
MMP7
C
Ad-shlacZ
Ad-shKLF11
Ad-shlacZ+TNF-α
Ad-shKLF11+TNF-α
P < 0.0001
Relative mRNA level
MMP2
MMP3
MMP9
MMP13
MMP14
D
Ad-GFP
Ad-KLF11
Ad-GFP+TNF-α
Ad-KLF11+TNF-α
P < 0.0001
Relative mRNA level
E
Control
TNF-α
100kDa
75kDa
pro-MMP9
active-MMP9
pro-MMP2
Ad-shlacZ
Ad-shKLF11
F
Control
TNF-α
100kDa
75kDa
pro-MMP9
active-MMP9
pro-MMP2
Ad-GFP
Ad-KLF11
G
MMP9 promoter
-594 cattccttCCGCCCCCagatg -574
P = 0.0018
Ratio of KLF11 binding/4% input
Ad-lacZ
Ad-flag-KLF11
IP:
IgG
anti-Flag
H
MMP9 698 bp promoter
P = 0.0034
Ad-lacZ
Ad-KLF11
Relative luciferase activity/Renilla
Control
TNF-α

1

Figure 4. KLF11 inhibits MMP9 expression and activity in endothelial cells. A-B. Human aortic endothelial cells (HAECs) were infected with adenovirus carrying-short hairpin RNA for *KLF11* knockdown (Ad-sh*KLF11*, 10MOI, n=4) or lacZ (Ad-sh*lacZ*, n=3) as control. After 48h, the total RNA was extracted for RNA sequencing. **A**. The positive enrichment in the membrane protein proteolysis and metalloexopetidase activity pathways is shown by GSEA plots (Ad-sh*KLF11* vs. Ad-sh*lacZ*). NES, normalized enrichment score. **B**. The differentially expressed genes (Ad-sh*KLF11* vs. Ad-sh*lacZ*) are shown as volcano plots. Green dots, log2FoldChange< -0.5. Red dots, log2Fold Change>0.5. Grey dots, -0.5<log2FoldChange<0.5. **C-F**. HAECs were infected with Ad-sh*lacZ*, Ad-sh*KLF1*1 for *KLF11* or Ad-*GFP*, Ad-*KLF11* (10 MOI). After 48h, they were treated with or without TNF-α (2 ng/ml) for 12h. **C**-**D**. The mRNA levels of *MMP2*, *MMP3*, *MMP9*, *MMP13*, *MMP14* were determined by qPCR. **E**-**F**. Representative gelatin zymography for the activity of MMP2 and MMP9 in the conditioned medium. Samples from E and F were run on 8% and 10% SDS-PAGE gels with 0.1% gelatin, respectively. **G**. HAECs were infected with Ad-*lacZ*, or Ad-flag-*KLF11*. After 48h, they were stimulated with TNF-α (2ng/ml) for 4h. Chromatin immunoprecipitation (ChIP) assay was performed using an antibody against flag or IgG. **H**. Luciferase reporter assay in HAECs transfected with an *MMP9* promoter-driven luciferase reporter containing a KLF11 binding site and infected with Ad-*lacZ* or Ad-*KLF11*. After 48h, they were stimulated with TNF-α (2 ng/ml) for 4h. The luciferase activity was normalized against that of co-transfected *Renilla*. Data are presented as mean±SEM. Two-way ANOVA followed by Holm-Sidak post hoc analysis for C-D, G-H.

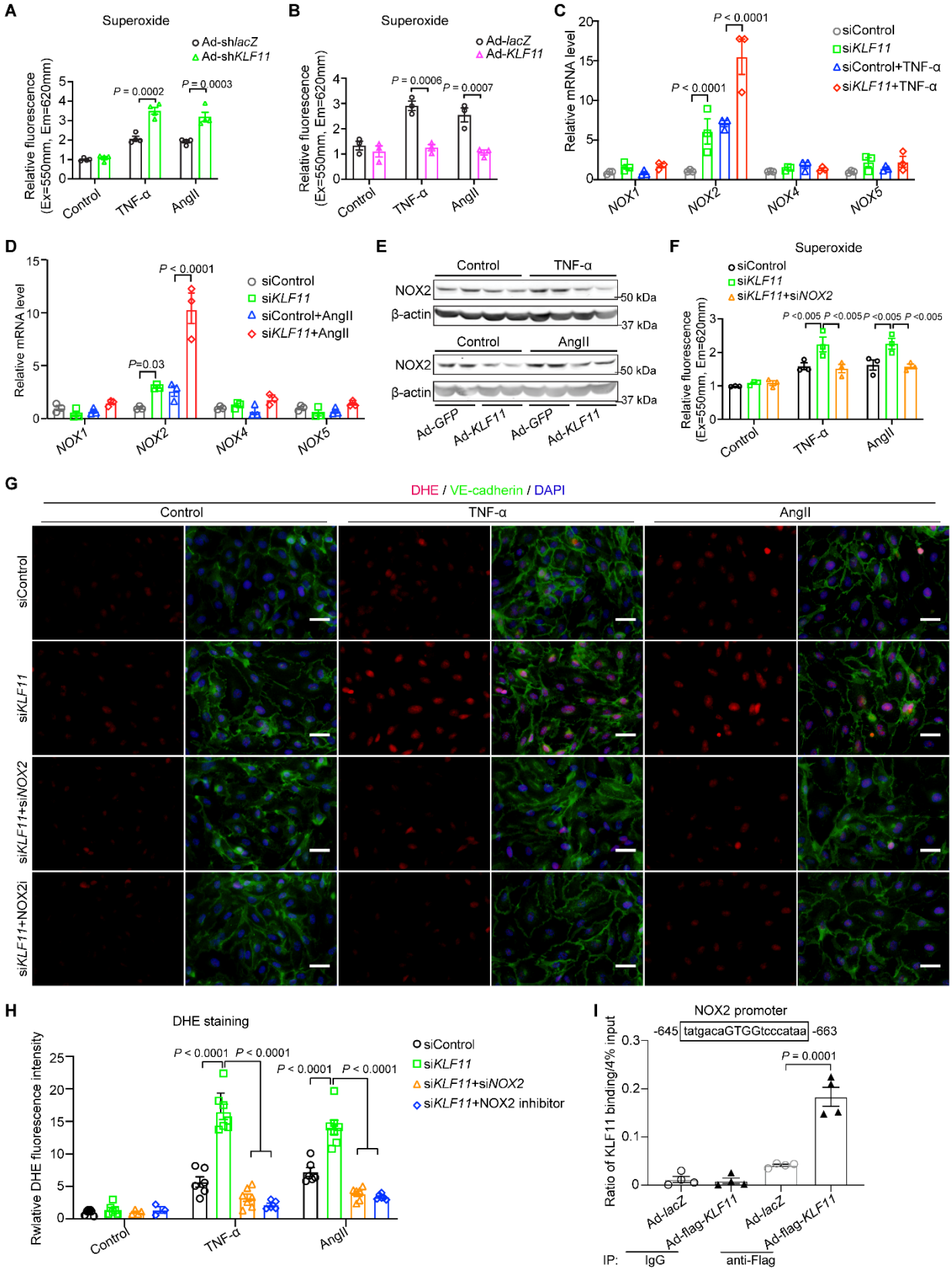
A
Superoxide
Ad-shlacZ
Ad-shKLF11
Relative fluorescence (Ex=550mm, Em=620mm)
P = 0.0002
P = 0.0003
Control
TNF-α
AngII
B
Superoxide
Ad-lacZ
Ad-KLF11
Relative fluorescence (Ex=550mm, Em=620mm)
P = 0.0006
P = 0.0007
Control
TNF-α
AngII
C
Relative mRNA level
P < 0.0001
P < 0.0001
siControl
siKLF11
siControl+TNF-α
siKLF11+TNF-α
NOX1
NOX2
NOX4
NOX5
D
Relative mRNA level
P < 0.0001
P=0.03
siControl
siKLF11
siControl+AngII
siKLF11+AngII
NOX1
NOX2
NOX4
NOX5
E
Control
TNF-α
NOX2
β-actin
50 kDa
37 kDa
Control
AngII
NOX2
β-actin
50 kDa
37 kDa
Ad-GFP
Ad-KLF11
Ad-GFP
Ad-KLF11
F
Superoxide
siControl
siKLF11
siKLF11+siNOX2
Relative fluorescence (Ex=550mm, Em=620mm)
P <0.005 P <0.005 P <0.005 P <0.005
Control
TNF-α
AngII
G
DHE / VE-cadherin / DAPI
Control
TNF-α
AngII
siControl
siKLF11
siKLF11+siNOX2
siKLF11+NOX2i
H
DHE staining
Rwlative DHE fluorescence intensity
P < 0.0001 P < 0.0001
P < 0.0001 P < 0.0001
siControl
siKLF11
siKLF11+siNOX2
siKLF11+NOX2 inhibitor
Control
TNF-α
AngII
I
NOX2 promoter
-645 tatgacaGTGGtcccataa -663
P = 0.0001
Ratio of KLF11 binding/4% input
Ad-lacZ
Ad-flag-KLF11
Ad-lacZ
Ad-flag-KLF11
IP:
IgG
anti-Flag

1

Figure 5. KLF11 attenuates ROS production through NOX2 suppression. A-B. The production of superoxide was determined in HAECs. HAECs were infected with Ad-*lacZ*, Ad-*KLF11* or Ad-sh*lacZ*, Ad-sh*KLF11* (10MOI). After 48h, they were treated with TNF-α (2ng/ml) or AngII (1μM) for 2h in the presence of superoxide detection solution (fluorescent probes). **C**-**E**. HAECs were infected with Ad-*GFP*, Ad-*KLF11* (10MOI) or transfected with control siRNA (siControl), *KLF11* siRNA (si*KLF11*, 20μM). After 48h, they were stimulated with TNF-α (2ng/ml) or AngII (1μM) for 24h. **C**-**D**. The mRNA levels of *NOX1*, *NOX2*, *NOX4* and *NOX5* were determined by qPCR. **E**. Western blot to determine the expression of NOX2 in HAECs. **F**. HAECs were transfected with siControl, si*KLF11* or si*KLF11*+*NOX2* siRNA (si*NOX2*) (20μM). After 48h, they were treated with TNF-α (2ng/ml) or AngII (1μM) for 2h in the presence of superoxide detection solution. **G**-**H**. Representative DHE staining and quantification of superoxide production in HAECs. HAECs were transfected with siControl, si*KLF11*, si*KLF11*+si*NOX2*. After 48h, they were pre-treated with NOX2 inhibitor (NOX2i, GSK2795039, 1μM) for 1h, and then stimulated with TNF-α (2ng/ml) or AngII (1μM) for 2h, followed by DHE staining of superoxide (red) and immunofluorescence staining of VE-cadherin (green). Nuclei stained by DAPI are blue. Scale bar=20μm. **I**. HAECs were infected with Ad-*lacZ* or Ad-flag-*KLF11*. After 48h, they were stimulated with TNF-α (2ng/ml) for 4h, followed by ChIP assay using an antibody against flag or IgG. Data are presented as mean±SEM. Two-way ANOVA followed by Holm-Sidak post hoc analysis for A-D, F and H-I.

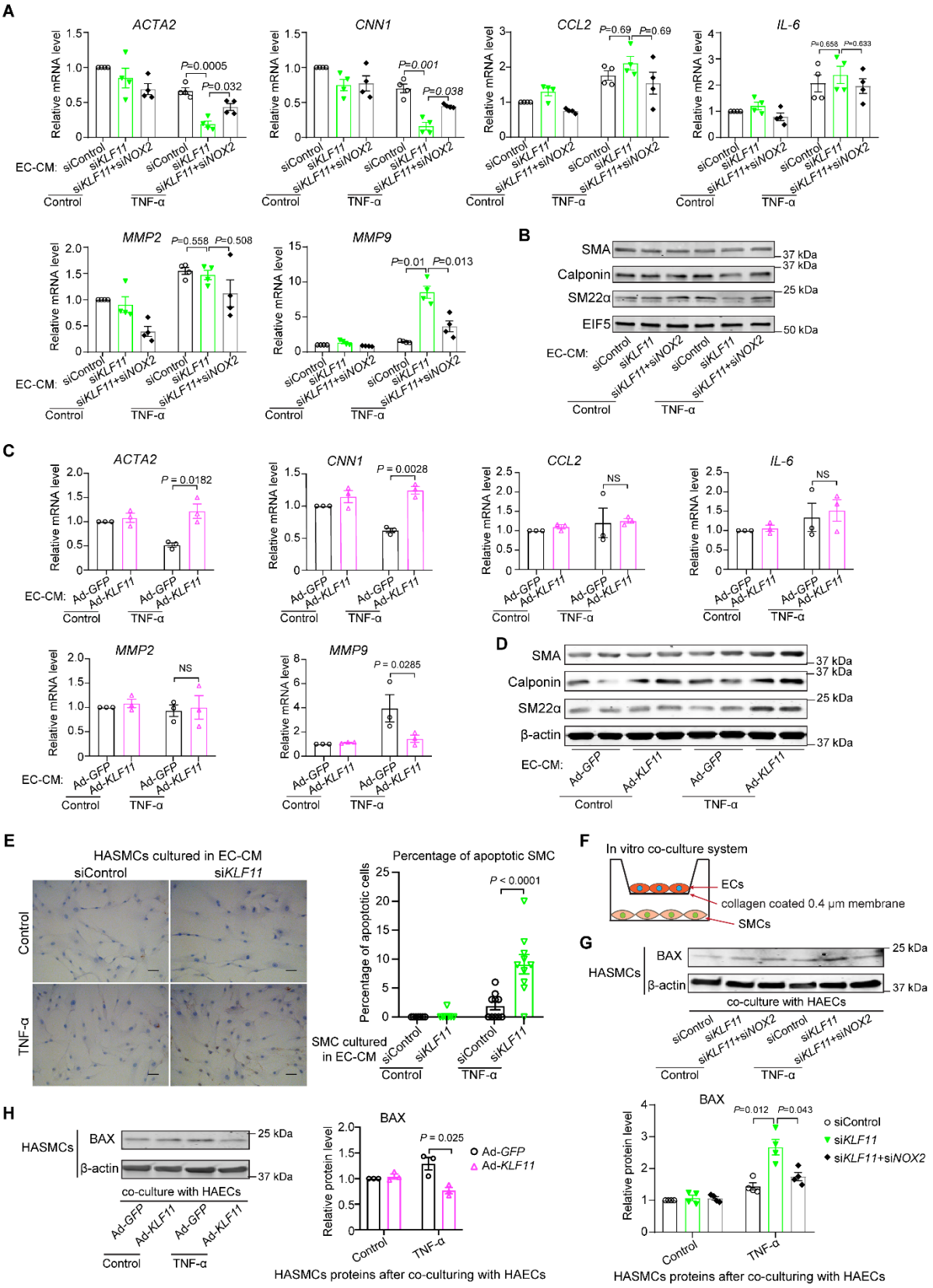
A
ACTA2
CNN1
CCL2
IL-6
MMP2
MMP9
Relative mRNA level
EC-CM: siControl siKLF11 siKLF11+siNOX2
Control
TNF-α
B
SMA
Calponin
SM22α
EIF5
37 kDa
25 kDa
50 kDa
C
Ad-GFP
Ad-KLF11
NS
D
β-actin
E
HASMCs cultured in EC-CM
siControl
siKLF11
Percentage of apoptotic SMC
Percentage of apoptotic cells
SMC cultured in EC-CM
F
In vitro co-culture system
ECs
collagen coated 0.4 μm membrane
SMCs
G
HASMCs
BAX
co-culture with HAECs
H
Relative protein level
HASMCs proteins after co-culturing with HAECs
siKLF11+siNOX2

Figure 6. Co-culture with KLF11-deficient endothelial cells impairs smooth muscle cells homeostasis. A-E. Human aortic smooth muscle cells (HASMCs) were treated for 24h with the conditioned media from ECs (EC-CM) that had been transfected with siControl, si*KLF11*, si*KLF11*+si*NOX2* (20μM), or infected with Ad-*GFP*, Ad-*KLF11* (10MOI) and subsequently stimulated for 1h with TNF-α (2ng/ml) 48h after siRNA transfection or adenovirus infection and cultured in fresh opti-MEM for an additional 4h. **A-D**. qPCR (**A**, **C**) and Western blot (**B**, **D**) to examine expression of SMC-specific contractile markers (smooth muscle a-actin [SMA], calponin and smooth muscle 22 alpha [SM22α]), pro-inflammatory cytokines (MCP-1 and IL-6) and metalloproteinases (MMP2 and MMP9). **E**. HASMCs were cultured in EC-CM for 48h, followed by immunostaining of TUNEL. Scale bar=20μm. **F-H**. Schematics of the *in vitro* co-culture system using a transwell. HAECs (upper chamber) transfected with siControl, si*KLF11* (20μM), si*KLF11*+si*NOX2* or infected with Ad-*GFP*, Ad-*KLF11* (10MOI) were cultured for 48h followed by TNF-α (2ng/ml) stimulation for 1h separately from HASMCs, changed to fresh opti-MEM and then co-cultured with HASMCs (bottom) in fresh opti-MEM for 24h. The expression of BAX in HASMCs was assayed by Western blot (**G**, **H**). Data are mean±SEM from three independent experiments. Two-way ANOVA followed by Holm-Sidak post hoc analysis for A, C, E, G-H.